INFLUENCE OF GRASSLAND HETEROGENEITY ON LAND–ATMOSPHERE COUPLING

By

Kelly Logan

Submitted to the graduate degree program in the Department of Geography and Atmospheric Science and the Graduate Faculty of the University of Kansas in partial fulfillment of the requirements for the degree of Doctor of Philosophy.

Committee members

Dr. Nathaniel A. Brunsell, Chairperson

Dr. David B. Mechem

Dr. Daniel R. Hirmas

Dr. Jesse B. Nippert

Dr. Randy L. Stotler

Date defended: April 27, 2018

The Dissertation Committee for Kelly Logan certifies
that this is the approved version of the following dissertation :

INFLUENCE OF GRASSLAND HETEROGENEITY ON LAND–ATMOSPHERE COUPLING

Dr. Nathaniel A. Brunsell, Chairperson

Date approved: April 27, 2018

Abstract

Land surface processes and interactions with the atmosphere have been identified as a weak point in our understanding of the Earth's climate system and contribute to uncertainty in projections of future climate. This weakness is due, in part, to the inherent complexity of land–atmosphere (LA) interactions and the highly heterogeneous nature of land cover across a variety of spatial and temporal scales. The research included in this dissertation looks at the significance of these issues over a central US grassland. Influence of spatiotemporal variability is investigated through comparison between two proximate grassland sites with differing land cover. High-frequency observations from eddy covariance towers over a study period covering a range of environmental forcings, including two strong droughts and woody encroachment at one site provides a unique opportunity for study. First, changes in the water, energy, and carbon budgets are studied, with focus on the influence of woody encroachment on carbon sequestration, water-use efficiency, and drought response. How these changes manifest in the nature of turbulent fluxes, including at which spatial and temporal scales, are invested through deviations from similarity theory, quadrant analysis, and wavelet decomposition. Second, the nature of coupling between the land surface and atmosphere is studied by utilizing a variety of LA feedback metrics and analysis tools that allow for investigation of several steps in the LA feedback chain. This research includes the first use of some of these tools (self-organizing maps and mixing diagrams) in an study of this nature. Results indicate that woody encroachment increases resilience to drought due to changes in canopy structure and root access to soil moisture, and highlight the need to carefully consider scale and objective when selecting a metric of LA coupling.

Acknowledgements

I am very grateful for the support I received from a great many people that made this dissertation possible. Most especially, I thank my advisor, Dr. Nate Brunsell, for his insightful guidance and continual encouragement. I am also extraordinarily thankful to my committee members: Dr. David Mechem, Dr. Dan Hirmas, Dr. Jesse Nippert, and Dr. Randy Stotler, each of whom brings a unique perspective and has taught me a great deal. Many thanks as well to Dr. Joshua K. Roundy for generously providing data and expertise. I would also like to thank my colleagues in the KU biometeorology lab for support, both emotional and technical. Last but not least, I offer heartfelt thanks to my family and friends, especially to Teddy and Jack for their unconditional support.

This research was supported by the National Science Foundation EPSCoR Program (NSF EPS-0553722 and EPS-0919443) and KAN0061396/KAN0066263, NSF Long Term Ecological Research grant to the Konza Prairie (DEB-0823341), and through AmeriFlux core site funding from the US Department of Energy under a sub contract from DE-AC02-05CH11231.

Contents

1 Introduction **1**

1.1 Motivation 1

1.2 Research Questions and Objectives 2

1.3 Organization of the Dissertation 3

2 Influence of drought on growing season carbon and water cycling with changing land cover **5**

2.1 Introduction 5

2.2 Methods 8

2.2.1 Site description 8

2.2.2 Data 9

2.2.3 Analysis 9

2.3 Results and Discussion 13

2.3.1 Productivity and Water Use Efficiency 13

2.3.2 Applicability of Monin-Obukhov Similarity Theory 17

2.3.3 Changes in Turbulent Dynamics 18

2.3.4 Scales of Motion 19

2.4 Summary and Conclusions 25

3 Comparison of land-atmosphere coupling metrics using long-term eddy covariance measurements at heterogeneous grassland sites **28**

3.1 Introduction 28

3.1.1 Land atmosphere coupling defined 29

3.1.2 Metrics . . . 31
3.1.3 Motivation . . . 34
3.2 Methods . . . 36
3.2.1 Site description . . . 36
3.2.2 Coupling Metrics . . . 37
3.2.2.1 Feedback parameter . . . 38
3.2.2.2 Priestley-Taylor Ratio . . . 39
3.2.2.3 Coupling Drought Index . . . 39
3.2.3 Analysis tools . . . 40
3.2.3.1 Mixing diagrams . . . 40
3.2.3.2 Self-organizing maps . . . 41
3.3 Results . . . 42
3.4 Discussion . . . 55
3.5 Summary and Conclusions . . . 63

4 Conclusions **67**

4.1 Summary of Findings . . . 67
4.2 Summary of Contributions . . . 70
4.3 Recommendations for Future Work . . . 71

List of Figures

2.1 Total annual CO_2 flux (in -gC/m^2) for KON (gold) and K4B (blue) for each year of study. Vertical bars indicate 95% confidence interval derived by adding uncertainty due to random error and gapfilling using 10,000 bootstrap samples. 13

2.2 Calculated seasonal water use efficiency (-gC/kgH_2O) from flux data for March, April and May (MAM), June, July and August (JJA), and September, October and November (SON) in 2008 (blue), 2009 (green), and 2011 (gold) at KON (circles) and K4B (asterisks). Vertical bars indicate 95% confidence interval derived by adding uncertainty due to random error and gapfilling using 10,000 bootstrap samples. 14

2.3 Measured cumulative ET (mm) at KON (gold) and K4B (green) and Konza precipitation (mm, blue) in (a) 2008, (b) 2009, and (c) 2011. 15

2.4 Stress factor of water vapor transport over the growing season at K4B (blue) and KON (gold) for (a) 2008, (b) 2009, and (c) 2011. Values greater/less than zero represent sweeping/ejecting motions dominating flow. 18

2.5 Standardized wavelet power spectrum for each site over 2008 (blues) and 2011 (yellows). Scales at which spectra differ significantly ($p<0.01$) between years for KON and K4B are indicated with red and pink asterisks, respectively. Orange asterisks indicate significant difference between sites. Values below the dashed gray line are characteristic of white noise processes. 20

2.6 Boxplot of normalized cospectra of CO_2 and water vapor at KON (gold) and K4B (blue) in (a) 2008, (b) 2009, and (c) 2011. Scales at which cospectra mean differ significantly ($p<0.01$) between sites are indicated with red asterisks. Scales at which variance differs ($p<0.05$) between sites are indicated with pink asterisks. There is no significant difference between sites ($p<0.01$) at any scale in 2008 or 2009. 21

2.7 Five-day moving average of correlation of water vapor and CO_2 fluxes by wavelet scale, *s*, of 10 through 13 (corresponding to timescales of 51.2 - 409.6 s) at KON (left column) and K4B (right column) for 2008 (green) and 2011 (gold). Correlation varies significantly ($p<0.01$) between sites K4B and KON in 2011 only, at all four scales. Within sites, at KON there is a significant difference between 2011 and 2008 at all scales plotted, while K4B only varies significantly between these years at $s = 12$ and 13. Gaps in time series are indicative of series of three or more days which contained too many missing data points ($>0.5\%$) and were therefore excluded from the analysis. 22

2.8 One-week moving average of eddy diameter (m) of maximum scalar transport for 2008 (left), 2009 (middle), and 2011 (right) at KON (gold) and K4B (blue). Leaf area index as measured at KON for each year is also shown (green, right axis). . . . 23

3.1 Cumulative annual precipitation (in mm) observed at Konza LTER headquarters for 2008 through 2016. 43

3.2 Timeseries of daily Priestley-Taylor Ratio at KON (gold) and KFB (blue) over the growing seasons (April 1 - October 31) of 2008 through 2016. 44

3.3 Mean June, July, and August CDI over the central United States for select years of study, including two summers with drought, 2011 (a) and 2012 (b), and two summers, 2013 (c) and 2015 (d), with normal and high summer precipitation, respectively. Konza LTER location is marked with +. 46

3.4 Time series of 30-year average daily CDI at the study site (black), overlain with 7-day CDI in the years with highest (2008) and lowest (2012) precipitation in blue and orange dashed lines, respectively. 47

3.5 Mixing diagrams of 2008 - 2016 growing season mean diurnal latent and sensible heat fluxes at KON (circles) and KFB (triangles) for (a) two wet (blue) and drought (gold) years, (b) top (blue) and bottom (gold) 10^{th} percentile of PTR values, (c) top (blue) and bottom (gold) 10^{th} percentile of PTR, and (d) lowest (blue) and highest (gold) 10^{th} percentile of deviations from climatological mean CDI. Total daily flux are decomposed into surface and atmospheric component vectors, shown in dashed and dotted lines, respectively. Also included are the surface (β_{sfc}) and atmospheric (β_{atm}) Bowen ratios, and ratios of sensible ($A_H = H_{atm}/H_{sfc}$) and latent ($A_{LE} = LE_{atm}/LE_{sfc}$) heat fluxes. 48

3.6 Distribution within each SOM classification of (a) days since last precipitation event, (b) air temperature (°C), (c) vapor pressure deficit (kPA), (d) horizontal wind speed (ms^{-1}), and (e) net radiation (wm^{-2})as measured at KON (gold) and KFB (blue). 51

3.7 Average FBP value of days within each SOM classification. FBP does not differ significantly between sites or between SOM classes. 52

3.8 Average CDI value of days within each SOM classification. SOM classes in which CDI differs significantly ($p < 0.05$) from the mean CDI at KON/KFB are marked with a gold/blue asterisks and classes in which the distribution of CDI differs significantly between the sites are marked with a red asterisk. 52

3.9 Distribution within each SOM classification PTR at KON (gold) and KFB (blue). SOM classes in which PTR differs significantly ($p < 0.05$) from the mean at KON/KFB are marked with a gold/blue asterisks and SOM classes in which the distribution of PTR differs significantly between the sites are marked with a red asterisk. 53

3.10 Mixing diagrams of mean diurnal development at KON (circles) and KFB (triangles) for select SOM classes: class 6 (teal) and class 8 (purple) in (a); class 7 (dark red) and class 9 (orange) in (b). Total daily flux are decomposed into surface and atmospheric component vectors, shown in dashed and dotted lines, respectively. Also included are the surface (β_{sfc}) and atmospheric (β_{atm}) Bowen ratios for each site and class. 54

Chapter 1

Introduction

1.1 Motivation

Land surface processes and interactions with the atmosphere have been identified as a weak point in regional climate models, with representation of surface fluxes in climate models critically affecting predicted near-surface climate over land (Davin et al., 2016). Unfortunately, current land-surface models (LSM) have been shown to perform no better at reproducing observed latent and sensible heat fluxes than empirical, regression-based statistical models (Davin et al., 2016; Abramowitz, 2012; Best et al., 2015). The lack of energy conservation in the observations from eddy-covariance (EC) tower has been demonstrated not to be the root cause of under-performance by LSM (Haughton et al., 2016). Rather, the partitioning of total energy between latent and sensible fluxes seem to be at issue.

This weakness is due, in part, to the inherent complexity of land–atmosphere (LA) interactions and the difficulty in observing some of the necessary variables (Santanello et al., 2017). Additionally, land surface properties are highly heterogeneous across a range of spatiotemporal scales (e.g. Betts, 2004; Ek & Holtslag, 2004; Reen et al., 2014). The surface heterogeneity is often overlooked for simplicity, but has been demonstrated to cause pronounced changes in the partitioning of surface energy (Brunsell et al., 2011).

Many metrics have been developed to appraise surface interactions with the planetary boundary layer (PBL). Particular interest has been paid to identifying "hotspots" of strong LA coupling (e.g. Koster et al., 2006; Notaro, 2008; Zhang et al., 2008; Zeng et al., 2010; Ferguson & Wood, 2011). The accuracy of these metrics is frequently assessed based on single-variable comparisons which

do not assess causality and can conflate compensating errors, thereby potentially overestimating accuracy (Santanello et al., 2017). Additionally, there is often disagreement between metrics. In particular, the Central Great Plains were originally identified as a prominent "hotspot" by Koster et al. (2006), but later studies have demonstrated strong disagreement on whether this area actually does display a particularly strong influence of local land-surface conditions on PBL growth or precipitation likelihood.

The Central Great Plains area is natively covered in grasslands. Grasslands have been shown to be especially sensitive to amount and timing of precipitation (Knapp et al., 2001, 2008; Blair et al., 2013). Productivity of grasslands change vary greatly with increasing aridity, sometimes even changing from a net sink to a source of carbon, thus potentially exacerbating the effects of global climate change (Aires et al., 2008; Meyers, 2001). Other studies predict widespread, consistent increases in grassland productivity with climate change despite the predicted increases in aridity (Hufkens et al., 2016).

Over the last century grasslands worldwide have been experiencing transformations to increased herbaceous and woody plant dominance (Blair et al., 2013; Jackson et al., 2002). That trend of woody encroachment can result in large changes in the carbon, hydrological, and energy cycles (Ratajczak et al., 2012; Barger et al., 2011; Nippert & Knapp, 2007a; Huxman et al., 2005). Woody encroachment also increases the heterogeneity and variance of the land surface, which can alter energy partitioning in and of itself (Ratajczak et al., 2016; Brunsell et al., 2011). It is vital the understand how these grassland changes influence LA feedbacks in order to be able to accurately estimate changes in regional carbon and water budgets, and to predict the response of grassland ecosystems to a changing climate.

1.2 Research Questions and Objectives

The purpose of this dissertation research is to investigate the influence of changes in grassland composition on local LA interactions using observational data. In particular, the research utilizes long-term surface observations by eddy covariance on two closely-located native tallgrass prairies

experiencing differing levels of woody encroachment. By comparing sites that receive similar climate forcings, this research aims to isolate the effect of small-scale, local heterogeneity on LA interactions – from changes in the structure of turbulence to the overall effect on carbon, water, and energy budgets.

Specifically, in order to assess the possible consequences of changing climate in the region and to diagnose potential causes of the aforementioned problems in estimation of LA coupling strength, this research aims to answer several questions:

- How does woody encroachment on grasslands affect ecosystem resiliency, particularly in response to increasing aridity and drought?
- How do these changes in vegetation alter surface energy partitioning and the structure of fluxes?
- Given the large discrepancies between LA coupling metrics in this area, which metrics most accurately assess LA feedbacks at the study sites?
- Do the differences in species' composition alone significantly alter LA coupling strength between the sites? And, if so, how does this heterogeneity affect the accuracy and utility of the coupling metrics?

1.3 Organization of the Dissertation

The overarching topic of the effects of changing grasslands on LA coupling are explored in two detailed studies. Chapter 2 provides an analysis of the influence of woody encroachment on local turbulent dynamics and the ramifications of those changes on the LA exchange of water and carbon. Chapter 3 investigates the effect of these land cover changes on the surface energy fluxes and interaction with the boundary layer through a variety of LA coupling metrics, also assessing the utility and suitability of the metrics to the region given the heterogeneous nature of the grasslands.

Each of these chapters are formatted as a journal article with an introduction addressing the specific problems and objectives, a methodology describing the data sources and analysis methods for that portion, results and discussion detailing findings of that study, and a conclusion section summarizing the chapter and describing how it fits into current scientific research. Lastly, Chapter 4 provides a brief summary of the overall conclusions drawn from this research and the contributions to the field of LA interactions.

Chapter 2

Influence of drought on growing season carbon and water cycling with changing land cover

2.1 Introduction

Over the last century grasslands have been experiencing transformations to increased herbaceous and woody plant dominance worldwide (Blair et al., 2013; Jackson et al., 2002). Grasslands, which make up the native vegetation of up to 40% of the global land cover, have been shown to be particularly sensitive to changes in precipitation amount and timing (Knapp et al., 2001, 2008; Blair et al., 2013). The trend of woody encroachment can result in large shifts in the carbon and hydrological cycles (Barger et al., 2011; Jackson et al., 2002; Huxman et al., 2005). Drought frequency and severity is expected to increase globally with climate change (Dai, 2012) and regional changes in ecosystem composition may alter the impact of these events through changes in ecosystem productivity, water use efficiency (WUE), and flux dynamics.

Grassland productivity is strongly linked to precipitation amount, and many studies have shown decreases in the magnitude of grassland carbon sequestration with decreased precipitation both globally and regionally in the central/western U.S. (Schwalm et al., 2010; Bowling et al., 2010). In fact, a shift from net carbon sink to source occurs with drought in many grasslands (Aires et al., 2008; Meyers, 2001). Management strategies and the resulting changes in species' composition alter carbon sequestration and drought response, with woody plants linked to increased Net Ecosystem Production (NEP) and lower sensitivity of NEP to precipitation variability, likely because encroaching woody C_3 plants tend to have root access to deeper sources of moisture (Rata-

jczak et al., 2012; Barger et al., 2011; Scott et al., 2006; Potts et al., 2006; Jurena & Archer, 2003). Annual burning of prairies has been shown to increase carbon losses to the atmosphere (Bremer & Ham, 2010) and lower WUE when compared to less frequent burn regimes that are more prone to woody encroachment (Brunsell et al., 2014). Changes in species' composition also alter canopy structure and patchiness of the land surface, which are expected to impact the effective surface roughness (Bou-Zeid et al., 2004). These changes may, in turn, alter the strength and structure of sensible and latent heat fluxes (Brunsell et al., 2011). Few studies have investigated in detail the differences in turbulent dynamics caused by the change in ecosystem composition.

Long-term surface observations by eddy covariance on natural prairies experiencing differing levels of woody encroachment offer unique insight into ecosystem-level changes. Two towers at the Konza Long Term Ecological Research Program (Konza LTER), located less than a mile apart in grasslands managed with different burn frequencies, provide the opportunity for investigation of the influence of species' composition on the carbon, water, and energy cycles under a variety of climate conditions while limiting the influence of regional climate variations such as boundary layer height or precipitation timing. This study aims to quantify that influence on Net Ecosystem Exchange (NEE) and WUE in years with and without drought conditions. In addition to changes in net fluxes, this study investigates how these vegetation shifts might affect boundary layer physics through changes in turbulent structure by using several tools: Monin & Obukhov (1954)'s Similarity Theory (MOST), quadrant analysis, and wavelet decomposition.

Deviations from MOST can be useful both in determining applicability of the theory under a variety of conditions and in pinpointing novel dynamics in the ASL. Williams et al. (2006) found that surface heterogeneity induced by seasonal onset of senescence, in an otherwise fairly homogeneous deciduous forest, results in increased deviations from MOST at the end of the growing season. Other studies have indicated dry soil moisture conditions can cause the failure of MOST in savanna and patchy tree-covered landscapes (Moene & Schüttemeyer, 2008; Detto et al., 2008). It is hypothesized that a differential sensitivity to soil moisture conditions and response to drought between shrubs and grasses within the grassland sites result in increased heterogene-

ity of the source/sink distributions of temperature, CO_2, and water vapor that can be detected as increased deviations from MOST during drought.

Quadrant analysis is commonly used to investigate coherent patterns in flux motions (Antonia, 1981; Raupach et al., 1996; Finnigan, 2000; Francone et al., 2012). Changes in dominant quadrant, especially with respect to scalar transport, may correspond to changes in net fluxes such as greater carbon uptake with a denser canopy or canopy response to water stress in drought conditions (Katul et al., 1997). In the surface layer, the dominant motion depends on stability and canopy conditions. Under neutral conditions, sweeps and ejections are typically balanced, while under unstable conditions ejections dominate over sparse canopies and sweeps dominate over denser canopies (Katul et al., 2006, 2013). It is hypothesized that the ratio of sweeps and ejections will differ between a stable grassland and one experiencing significant woody encroachment with sweeps becoming more prominent with the resultant changes in canopy composition.

Wavelet analysis allows for differences in total fluxes to be broken down by scale of motion and eddy size (Farge, 1992). Correlation of wavelet coefficients of CO_2 and water vapor can be used to trace the source of fluxes at specific frequencies and points in the time series, and has been used effectively to partition evapotranspiration and to remove the effects of large advecting motions from the boundary layer (Scanlon & Albertson, 2001; Scanlon & Kustas, 2010). Differences in the scale of primary energy and scalar transport during wet and drought years will be investigated between sites using wavelet decomposition. To the best of our knowledge, wavelet decomposition has not been used extensively to investigate how the eddy diameter most effectively transporting canopy transpiration changes with different moisture regimes and over the course of the growing season.

Understanding just how regional changes in land cover alter drought response is vital for predicting future carbon and water cycling issues in response to climate change. Utilizing the many methods described above, this study aims to quantify differences in net carbon and water fluxes, flux efficiency and predictability, and dominant type and size of flux motion over the course of growing seasons between two sites over several years of interest that span a variety of moisture

regimes.

2.2 Methods

2.2.1 Site description

The two study sites are located less than a mile apart in the Konza LTER: a 3,487-ha native tallgrass prairie in northeastern Kansas, USA (39°N, 96°W). One site (KON) is located in an annually-burned (since 1978) watershed. The second site (K4B) is in a watershed that has prescribed burns every four years since 1975 (Brunsell et al., 2014). Burns are generally carried out in late April and both watersheds were burned in 2009. The prairies were both dominated by perennial C_4 grass species (*Andropogon gerardii, Panicum virgatum, Schizachyrium scoparium, Sorghastrum nutans*), until a recent explosive growth of dogwood (*Cornus drummondii*) at K4B. Fractional dogwood coverage was between about 30 and 55% at K4B during the study period, while forbs and woody plants remained less than 5% average coverage at KON.

Inherent variation among tower sites is a limitation for almost all studies of this nature, thus there are some potentially confounding differences between these study sites. The primary difference is that KON is located on an upland topographic area, while K4B tower is on a lowland watershed. Consequently, while the soil types are similar between sites, the soil at K4B is deeper, typically greater than 1.5 m, while the upland site has Florence limestone bedrock at less than 0.5 m (Nippert et al., 2011). However, the sites were selected for their long record, distinct recent shift in vegetation composition, and very close proximity. The short distance between sites ensures that they experience similar regional forcings. For instance, measured net radiation had a correlation of 0.96 between sites across all years of study, and soil temperature, continuously-measured at 8 cm depth, had a correlation of 0.99 between sites. The sites also experience nearly identical precipitation intensity and timing, receiving an average of 828 mm precipitation annually from 1983 to 2012. With the same regional forcings, observed differences between sites can be attributed primarily to management strategy and consequent vegetative composition.

This study spans two recent wet years (2008, 2009) and a drought year (2011) between prairie sites less than a mile apart. The sites received 1153 mm and 987 mm of precipitation in 2008 and 2009, respectively. These years were also cooler than the prairie's annual average of 12.7°C, with mean annual air temperatures of 11.7°C in 2008 and 11.9°C in 2009. During the drought year of 2011 the sites received 814 mm of precipitation and were warmer than usual, with a mean annual air temperature at 13.0°C. 2011 started moderately wet, but was followed by a much drier summer with many record-breaking high temperatures. In fact, heat wave indices show 2011 comparable to the highest recorded values outside of the 1930's (Karl et al., 2012).

2.2.2 Data

Data has been collected continuously since 2007 from two flux towers located 3 m above the surface. Temperature, water vapor and CO_2 concentrations, and three orthogonal components of wind velocity are measured continuously at 20 Hz using a triaxial sonic anemometer (CSAT-3; Campbell scientific, Logan, UT, USA) and an open-path gas analyzer (LI-7500; Li-Cor, Lincoln, NE, USA). In addition, local micro-meteorological stations measure meteorological variables within each watershed. Changes in canopy height and LAI of grasses were measured every two weeks throughout the growing seasons. CO_2 exchange and water vapor fluxes were calculated by the eddy covariance method. Meteorological convention of upward flux from the surface as positive was used. For seasonal analysis, high-frequency data was despiked with a moving window using a threshold of five times the standard deviation of data to remove erroneous outliers. For annual net ecosystem exchange (NEE) and seasonal WUE calculations, half-hourly sums were processed according to AmeriFlux standardized methods, and missing values were gapfilled (Reichstein et al., 2005).

2.2.3 Analysis

Total CO_2 fluxes over the years of interest were calculated for each site to determine how woody encroachment changes the magnitude of the carbon sink, and whether the sites become a CO_2

source during drought years. For consistency with end-of-season aboveground biomass observations, annual NEE is summed from half-hourly flux measurements starting on November 1st of the prior year and ending on October 31st, considered the end of the growing season, of the year of interest. WUE was calculated seasonally as the change in carbon assimilation (A) over water flux (LE): $WUE = dA/dLE$, where $A = NEE - R_{eco}$, where the ecosystem respiration, R_{eco}, was calculated as shown in Brunsell et al. (2014). Gapfilling accounted for a total of around 10% of the annual fluxes at both sites in 2008, 8% and 12% in 2009, and 33% and 30% in 2011 for K4B and KON, respectively, with the majority of gapfilling in 2011 occurring outside of the growing season. Errors in annual NEE and seasonal WUE associated with this gapfilling and with random measurement error were derived using 10,000 bootstrap samples with random noise added and the original percentage of missing data introduced and subsequently gapfilled (Moncrieff et al., 1996; Wohlfahrt et al., 2005).

For analysis of turbulent structure, high-frequency (20Hz) observations were used from daytime periods (10am to 4pm) covering the growing seasons (April 1st through October 31st). Despiked or missing data points in the high-frequency observation were linearly filled. However, to minimize the influence of this gapfilling, only daytime periods with less than 0.5% of observations filled were used. Stability of each half-hourly period of the high-frequency data was classified according to MOST, using $\zeta = (z - d_o)/L_o$, where z is the height of observation (m), d_o is the zero-plane displacement, calculated at 75% of the height of the canopy (Foken, 2006). L_o is the Obukhov length, defined as:

$$L_o = \frac{-u_*^3 \overline{T_v}}{kgH}, \tag{2.1}$$

where $\overline{T_v}$ is the half-hour average virtual temperature (K), H is the half-hour kinematic heat flux (K m s^{-1}), k is the Von Karman constant (0.41), g is gravitational acceleration (9.81 m s^{-1}), and u_* is frictional velocity (m s^{-1}), calculated as:

$$u_* = [(\overline{u'w'})^2 + (\overline{v'w'})^2]^{1/4}, \tag{2.2}$$

with turbulent fluctuations u', w', and v' about the half-hourly mean wind velocities. Observations under near-neutral ($-0.1 < \zeta < 0$) and unstable ($\zeta < -0.1$) conditions were used for this analysis. Additionally, a threshold u_* value (> 0.1) was used for analysis to ensure appropriate application of Taylor's frozen turbulence hypothesis.

Under free convection conditions, normalized standard deviations (σ_s/s_*, with $s_* = \overline{w's'}/u_*$) of any scalar, s, are expected to increase with increasing instability according to a power law ($-\zeta^{-1/3}$) if all MOST conditions are met: stationarity, horizontal homogeneity, and lack of boundary layer influence (above the surface layer) (Cava et al., 2008; Williams et al., 2006; Wyngaard et al., 1971). The transport efficiency ratio, defined as the ratio of correlation coefficients between vertical velocity and scalars $r_{ws} = \overline{w's'}/(\sigma_w\sigma_s)$, should also approach ± 1 with decreasing stability. Variance of deviations from MOST were calculated for each growing season to detect a difference between sites due to differences in surface heterogeneity. One-week moving average of deviations from MOST were calculated in a manner similar to Williams et al. (2006) in order to determine if there is detectable an increase in deviations with onset of drought at either site.

A simple quadrant analysis of winds, using a Cartesian plane with vertical winds (w) and latitudinal winds (u) as the ordinate and abscissa, respectively, was used to determine dominant form of motion of turbulent atmospheric motions. Ejections are instantaneous deviation from the mean velocity (denoted with $'$) in quadrant 2 of the plane ($u' < 0$, $w' > 0$) and sweeps are defined as motions in quadrant 4 ($u' > 0$, $w' < 0$). The net contribution is measured by the stress factor, $S_i = \frac{\overline{u'w'}_i}{\overline{u'w'}}$, where $\overline{u'w'}_i$ is the flux in quadrant i and $\overline{u'w'}$ is the total flux. Imbalance in contributions from sweeps and ejections is defined by Nakagawa & Nezu (1977) as the difference of stress factors for these quadrants:

$$\Delta S_0 = \frac{\overline{u'w'}_4 - \overline{u'w'}_2}{\overline{u'w'}}. \tag{2.3}$$

ΔS_0 varies between -1 and 1, provided total momentum flux is not 0. Sweeps dominate transfer when $\Delta S_0 > 0$ and ejections dominate when $\Delta S_0 < 0$. The mean and distribution of ΔS_0 between sites and years was compared for statistically significant differences. Changes over the growing seasons were investigated using simple linear regression. Both scalar transport (CO_2 and water

vapor) and momentum transport were investigated in this manner.

Differences in scale of primary energy or scalar transport between wet and drought years and between sites was investigated using wavelet decomposition. Discrete wavelet transformation (DWT), rather than continuous, was chosen to avoid redundant information. The Haar wavelet, the simplest possible basis, was selected for the turbulent flux data analysis because it controls for sharp discontinuities well, as it is more localized in the time domain than many of the more complex wavelet bases (Falge et al., 2001). This basis has been shown to be a good identifier of turbulent energy in the wavelet domain (Scanlon & Albertson, 2001). DWT was performed on 6-hour midday time series of vertical wind, water vapor, carbon, and heat fluxes. The analysis requires a complete time series, so despiked or missing data points were linearly filled. To minimize the influence of this gapfilling, only days with less than 100 seconds of missing data, or less than 0.5% of the daily duration analyzed, were used. Each time series was padded with zeros to the nearest 2^M data points, and wavelet transformation was applied to the dyadic time series, resulting in 2^{M-m} wavelet coefficients (WC) at each scale, m, where $m = 1, 2, ..., M$. WC within the cone of influence were removed. Resulting WC are analogous to perturbation terms specific to each scale (Scanlon & Albertson, 2001).

The power spectral density function was computed by taking the time average of squared WC and standardizing by scale. The wavelet spectral density function represents the total energy contained at each scale. Wavelet cospectra are calculated in a similar manner, using WCs of two variables and normalizing with standard deviations of each, resulting in correlations between variables of interest at each scale. Using Taylor's hypothesis of frozen turbulence, scales can be converted to eddy diameter, d_m (m), calculated by:

$$d_m = \frac{2^m \overline{u}}{f_s}, \tag{2.4}$$

with f_s, the frequency of observation (s^{-1}), and $\overline{u}$, the mean horizontal wind speed. To determine the dominant eddy size of net fluxes, half-hourly sums of WC were calculated by scale and a

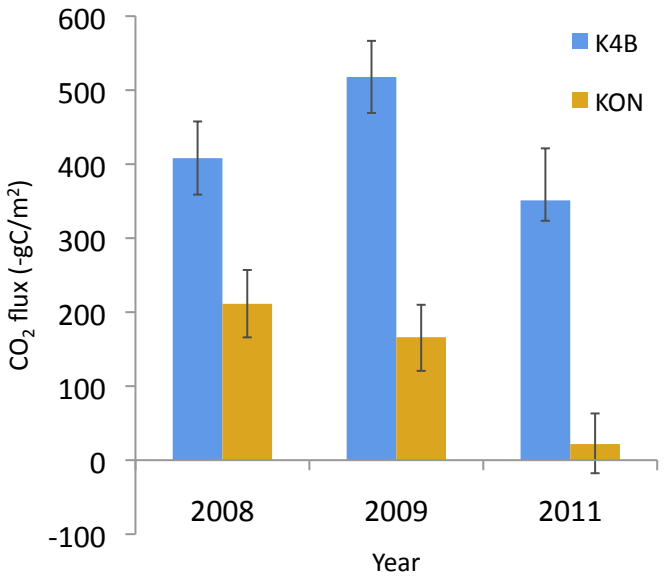

Figure 2.1: Total annual CO_2 flux (in -gC/m^2) for KON (gold) and K4B (blue) for each year of study. Vertical bars indicate 95% confidence interval derived by adding uncertainty due to random error and gapfilling using 10,000 bootstrap samples.

quadratic regression was fit with least squares error to determine the daily peak eddy diameter of water vapor, CO_2, and momentum fluxes.

2.3 Results and Discussion

2.3.1 Productivity and Water Use Efficiency

Evaluation of CO_2 fluxes over the span of the study shows a distinct decrease in productivity with the midseason drought onset in 2011. Figure 1 shows cumulative CO_2 flux at the sites for each year. Exact values of the sink are not known because the towers do not take measurements during burns, so upward flux of CO_2 from burning of aboveground biomass is not directly measured. However, the approximate magnitude of fluxes can be compared between levels of woody encroachment. Clearly, K4B is a significantly larger sink of carbon overall, with measured cumulative CO_2 fluxes 1.7, 3.2, and 7.2 times greater than KON in 2008, 2009, and 2011, respectively. To estimate the error from not measuring fluxes during burning, the carbon content of the previous year's end-

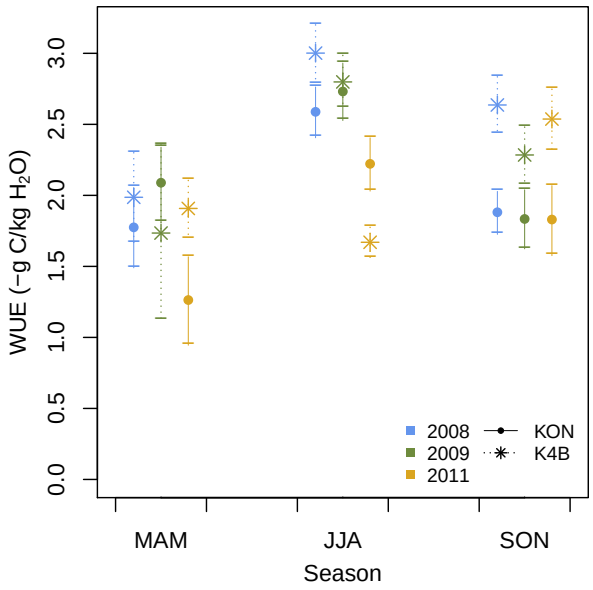

Figure 2.2: Calculated seasonal water use efficiency (-gC/kgH_2O) from flux data for March, April and May (MAM), June, July and August (JJA), and September, October and November (SON) in 2008 (blue), 2009 (green), and 2011 (gold) at KON (circles) and K4B (asterisks). Vertical bars indicate 95% confidence interval derived by adding uncertainty due to random error and gapfilling using 10,000 bootstrap samples.

of-season biomass clipping are used as a conservative maximum possible flux to the atmosphere that could result from spring burning. This missing component is not included in the cumulative NEE, but is added as additional error into the confidence interval in Figure 1. Carbon flux from burning in 2009 at K4B is estimated as a maximum of 43 gCm^{-2}, showing productivity at K4B is greatest when the site is burned. The site is a consistently large sink of carbon over all years of study, averaging -370 gCm^{-2} and remaining relatively unaffected by the drought of 2011. Net productivity at the annually burned grassland is much more variable and became almost negligible in 2011, at 37 gm^{-2} sink. When considering the additional error of carbon flux not included from annual burning, estimated at a maximum of 26 gCm^{-2}, the site becomes a possible source of carbon in the drought year, as seen through the wide confidence interval in Figure 1, extending into positive atmospheric flux for KON in 2011.

WUE given in negative grams of carbon per kg of water flux for spring, summer, and fall are shown in Figure 2. K4B had greater (more negative) efficiency in all periods except early 2009,

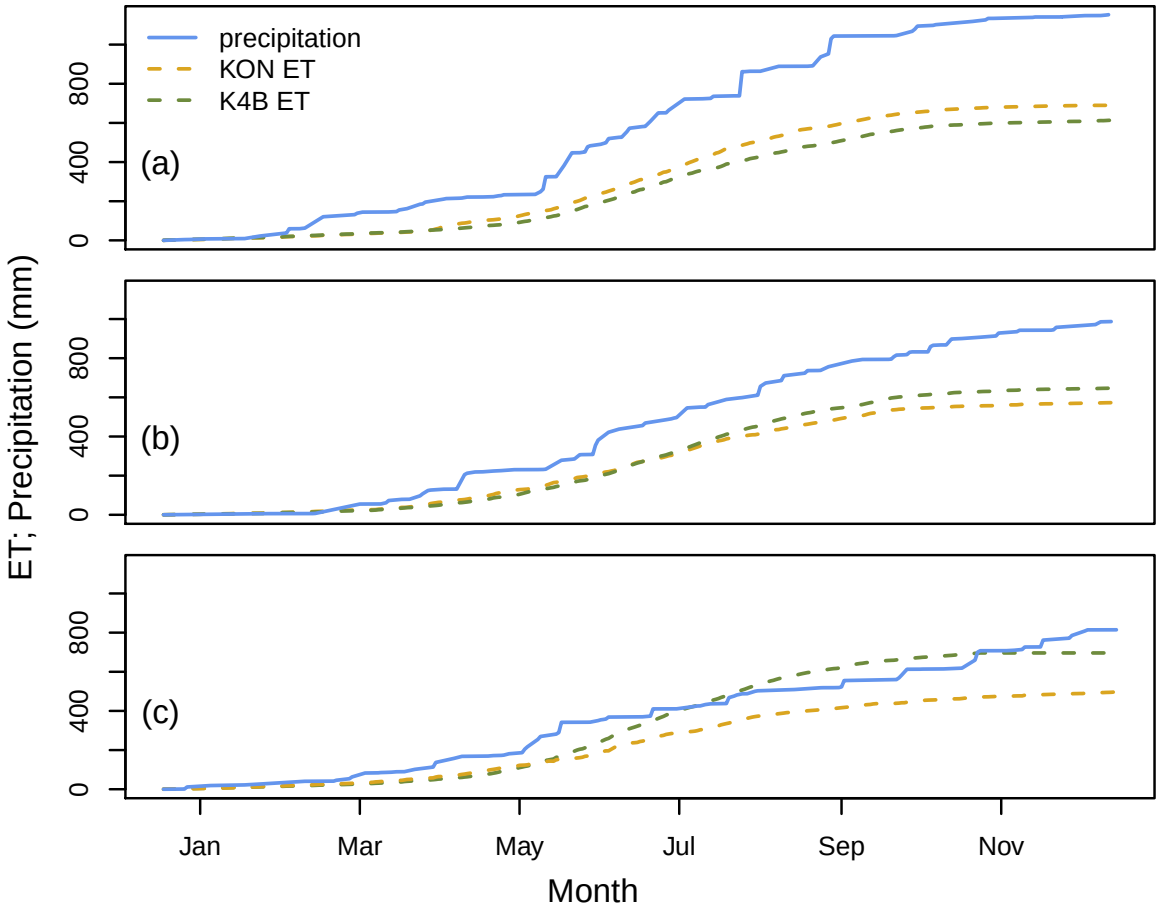

Figure 2.3: Measured cumulative ET (mm) at KON (gold) and K4B (green) and Konza precipitation (mm, blue) in (a) 2008, (b) 2009, and (c) 2011.

when the site was burned, and the summer of 2011, during which drought conditions persisted. A previous study by Brunsell et al. (2014) had shown that the site with woody encroachment has greater WUE, despite the higher leaf-level efficiency of C_4 plants. These results were confirmed for seasons with wet conditions, but did not hold with drought or in the season during and directly after a burn at the woody site. In the spring and summer after both sites were burned, the sites behaved similarly, with no statistically significant differences in WUE. This could be attributed to the rapid rebound of grasses, which would result in a more similar composition between sites for a brief period following the burns. It is hypothesized that the lack of response to 2011 summer drought is caused by root access to deeper sources of soil moisture in the encroaching shrubby plants. This could cause both the greater NEP and the lower WUE, as the plants are able to keep stomata more open without the same level of water stress as plants with shallower root access, but would also transpire much more water given the dry conditions.

Using stable isotope analysis, Ratajczak et al. (2011) has shown that the encroaching dogwood depends on deeper sources of soil moisture while the dominant prairie grasses rely on near-surface moisture. A comparison of the annual cumulative latent heat flux (converted to mm of upward water flux) against cumulative precipitation measurements appears to confirm these results (Figure 3). Beginning in June of 2011, precipitation decreased greatly, creating drought conditions soon after which remained in place for the rest of the growing season. While the ET rate at KON slowed in response, K4B continued transpiring at a similar (or greater) rate, resulting in a larger cumulative annual upward flux of moisture than received in precipitation. This clearly indicates that moisture for ET at this site must be drawn from sources other than recent precipitation events and near-surface moisture, likely deeper stored soil moisture.

2.3.2 Applicability of Monin-Obukhov Similarity Theory

Disparity between normalized standard deviations of flux efficiency from MOST predictions were investigated for each year at both stations to understand how woody encroachment and differing response to drought affect predictability of fluxes. Previous studies have shown increased dissimi-

larity with heterogeneous land cover and from seasonally induced increases in heterogeneity with senescence. While it was expected that the onset of patchy senescence at the end of the growing season would cause increased deviations from MOST predictions (e.g. Williams et al. 2006) that would occur earlier at the more drought-sensitive site during drought conditions, no significant changes over the growing seasons were found. It is possible that the heterogeneity of plant composition at the sites is similar to, or overwhelms the signal of any heterogeneity from patchy senescence. Normalized scalar standard deviations were often above MOST flux-variance predictions, and were more frequently so at K4B, where dogwood introduces more patchy heterogeneity to the landscape. Additionally, dissimilarity between predicted and observed normalized standard deviations of CO_2 and water vapor was highest at K4B in 2009, after the site had been burned. Established patches of Dogwood, the primary shrub at this site, have less herbaceous fuel at the edges than grasslands, allowing them to be more fire resistant and contain greater biomass immediately following a fire (Ratajczak et al., 2011). This effect seems to have led to a more heterogeneous landscape following the burn at K4B, somewhat weakening similarity applications in the roughness sublayer. Overall, turbulent fluxes at the sites generally conformed well with similarity theory.

2.3.3 Changes in Turbulent Dynamics

Ejecting and sweeping motions dominate net momentum and scalar transport. Quadrant analysis was used to find differences between sites in the primary type of motion. The imbalance of contributions by sweeps and ejections, ΔS_0, is shown in Figure 4. There was a significant difference ($p<0.01$) in mean ΔS_0 between sites every year, with sweeps more prominent in momentum transport at KON and ejecting motions from the canopy tending to be more dominant at K4B. Some studies have shown that ΔS_0 is higher with denser canopies (Katul et al., 2006, 2013), which would lead to an expectation of increasing ΔS_0 seasonally and higher ΔS_0 values at K4B, where LAI tends to be higher. However, results for momentum show the opposite, with ΔS_0 steadily lower at K4B and tending to decrease slightly over the growing season, corresponding to increased ejections from the canopy with greater canopy density. ΔS_0 of scalar transport displayed a similar pattern

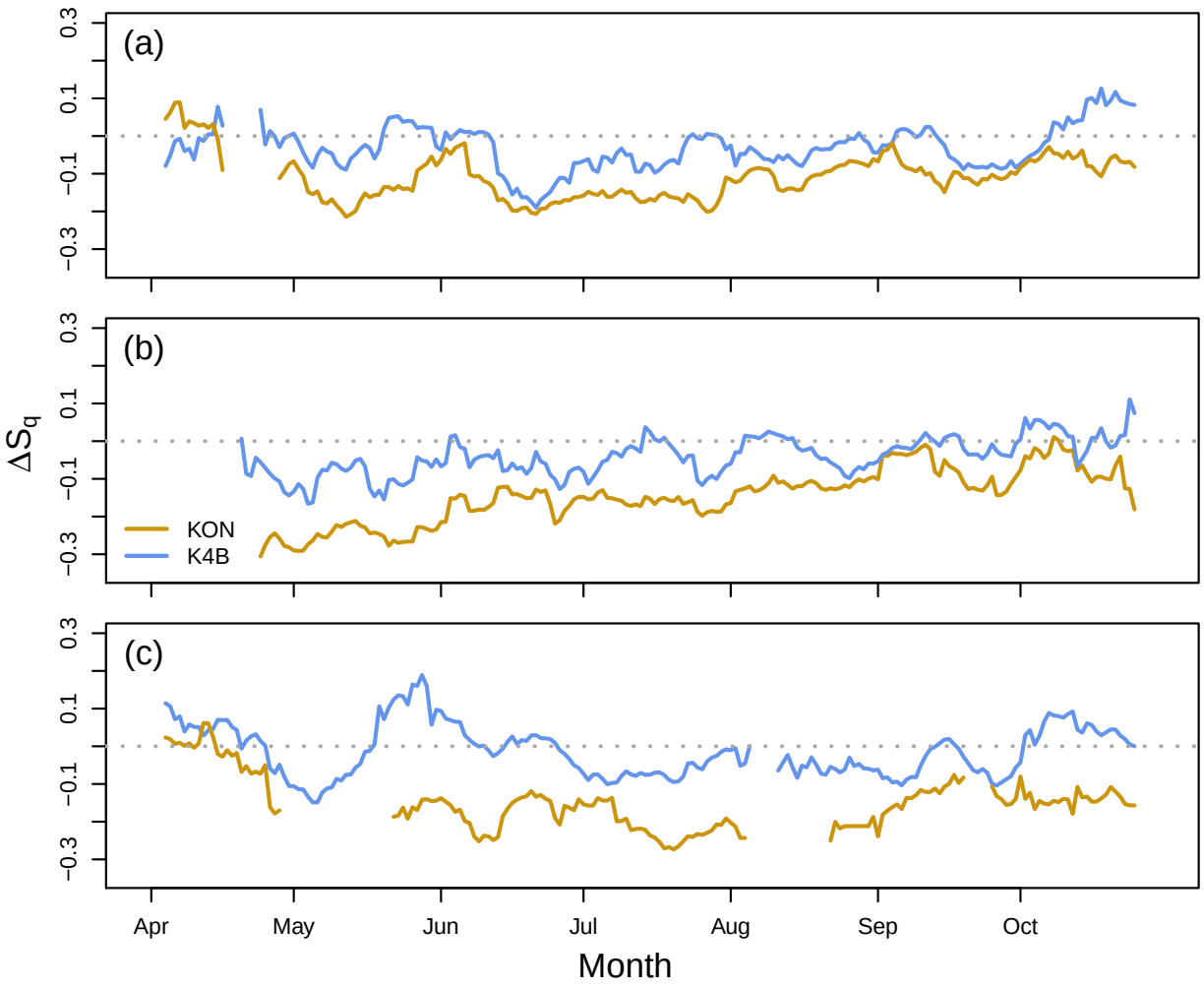

Figure 2.4: Stress factor of water vapor transport over the growing season at K4B (blue) and KON (gold) for (a) 2008, (b) 2009, and (c) 2011. Values greater/less than zero represent sweeping/ejecting motions dominating flow.

for the transport of water and CO_2. For each, values of scalar ΔS_0 were lower than for momentum. Ejecting motions dominated scalar transport over the growing seasons and ΔS_0 values were consistently higher at K4B (Figure 4). For scalar transport there was a statistically significant increasing trend in ΔS_0 seasonally at both sites in 2008 and 2009.

2.3.4 Scales of Motion

Wavelet decomposition was used to break down the time series into strength of total momentum and scalar flux across a range of frequencies. Figure 5 shows the standardized power spectrum of momentum for the sites in 2008 and 2011. The power spectra differed significantly between 2008 and 2011 at KON and K4B at small scales (1.6 to 3.2 s) and also at K4B for one large scale of 27.3 minutes. Because the larger scale represent only a few data points, uncertainty is higher. The smaller scales represent eddies of an average size of 5.9 to 12.8 m. Between sites, power spectra differ significantly across all scales except 0.8, 51.2, 102.4, and 204.8 s (s = 4, 10, 11, and 12). The higher scales with similar power between sites represent average eddy sizes of 180 m to 720 m. The similarity at these scales in terms of momentum may be indicative of the similar boundary layer forcings at the closely located sites. Differences between sites at the largest scales may be due to the inherent lack of data points at longer timescales over the 6-hour daily time series. The smallest scales (0.4s and lower) are characteristic of white noise processes and are not considered. Differences in scales from 1.6 to 25.6 seconds are thus believed to be attributable to differences between sites with woody encroachment, such as changes in canopy height (as measurement height stays constant), heterogeneity, and effective roughness. Relative to K4B, the grassland site contained less energy at these smaller scales, and more in the largest scales. This pattern is consistent across all years investigated. The cospectra for *wq* and *wc* are both significantly different between KON and K4B in 2011 at small scales (1.6 to 6.4 s), corresponding to eddy sizes of 5.9 to 23.6 m. This encompasses the eddy diameters of maximum CO_2 and water transport.

Normalized wavelet cospectra of CO_2 and water vapor are shown in Figure 6. These were nor-

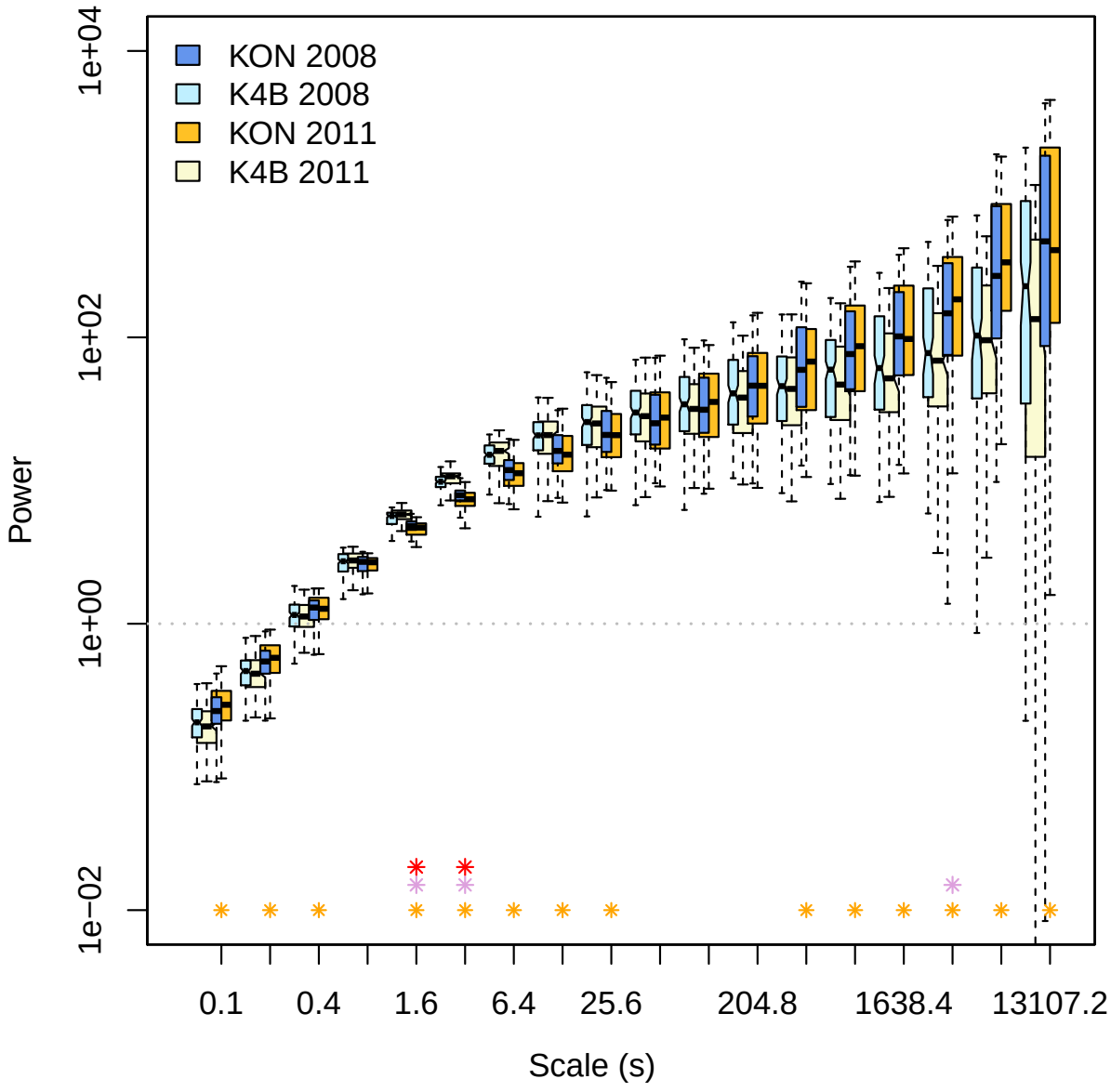

Figure 2.5: Standardized wavelet power spectrum for each site over 2008 (blues) and 2011 (yellows). Scales at which spectra differ significantly ($p<0.01$) between years for KON and K4B are indicated with red and pink asterisks, respectively. Orange asterisks indicate significant difference between sites. Values below the dashed gray line are characteristic of white noise processes.

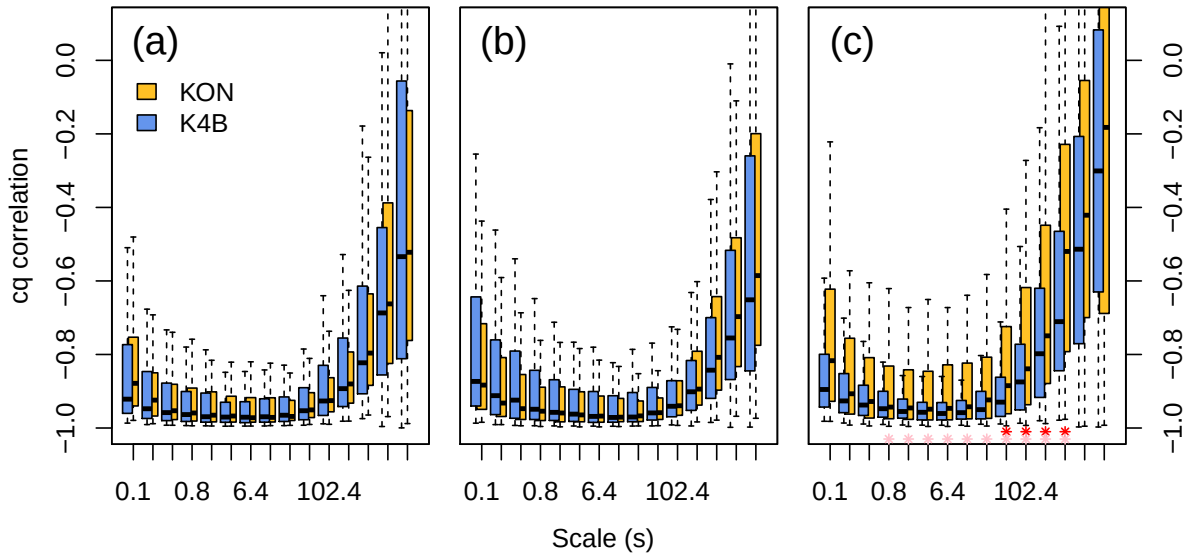

Figure 2.6: Boxplot of normalized cospectra of CO_2 and water vapor at KON (gold) and K4B (blue) in (a) 2008, (b) 2009, and (c) 2011. Scales at which cospectra mean differ significantly ($p<0.01$) between sites are indicated with red asterisks. Scales at which variance differs ($p<0.05$) between sites are indicated with pink asterisks. There is no significant difference between sites ($p<0.01$) at any scale in 2008 or 2009.

malized by scale-wise standard deviations, and represent *cq* correlations at each scale, *s*. Sources and sinks of CO_2 in the canopy are strongly coupled, as eddies containing air from active plants would be enriched in water and depleted in CO_2, causing a correlation near -1. As expected for the daytime observations during the growing season, the canopy dominated land-atmosphere water vapor and CO_2 exchanges, shown by a strong -1 correlation. Correlation of *cq* averaged close to -1 across nearly all scales, increasing to means greater than -0.8 only at scales of 102.6s and larger. There were no significant differences in *cq* correlations between sites in 2008 or 2009 and within each site there was no significant difference between 2008 to 2009. However, in 2011, the variance of correlations was much higher at KON across all scales, and there were significant differences between sites in *cq* correlations at medium to large scales (*s* of 10 to 13). At these scales there was also a significant change from 2008 to 2011 and 2009 to 2011 at KON. Differences between these years are also significant at K4B, but only for the larger *s* of 12 and 13. The time series of *cq* correlations by scale for these scales of interest (Figure 7) shows an early breakdown of the

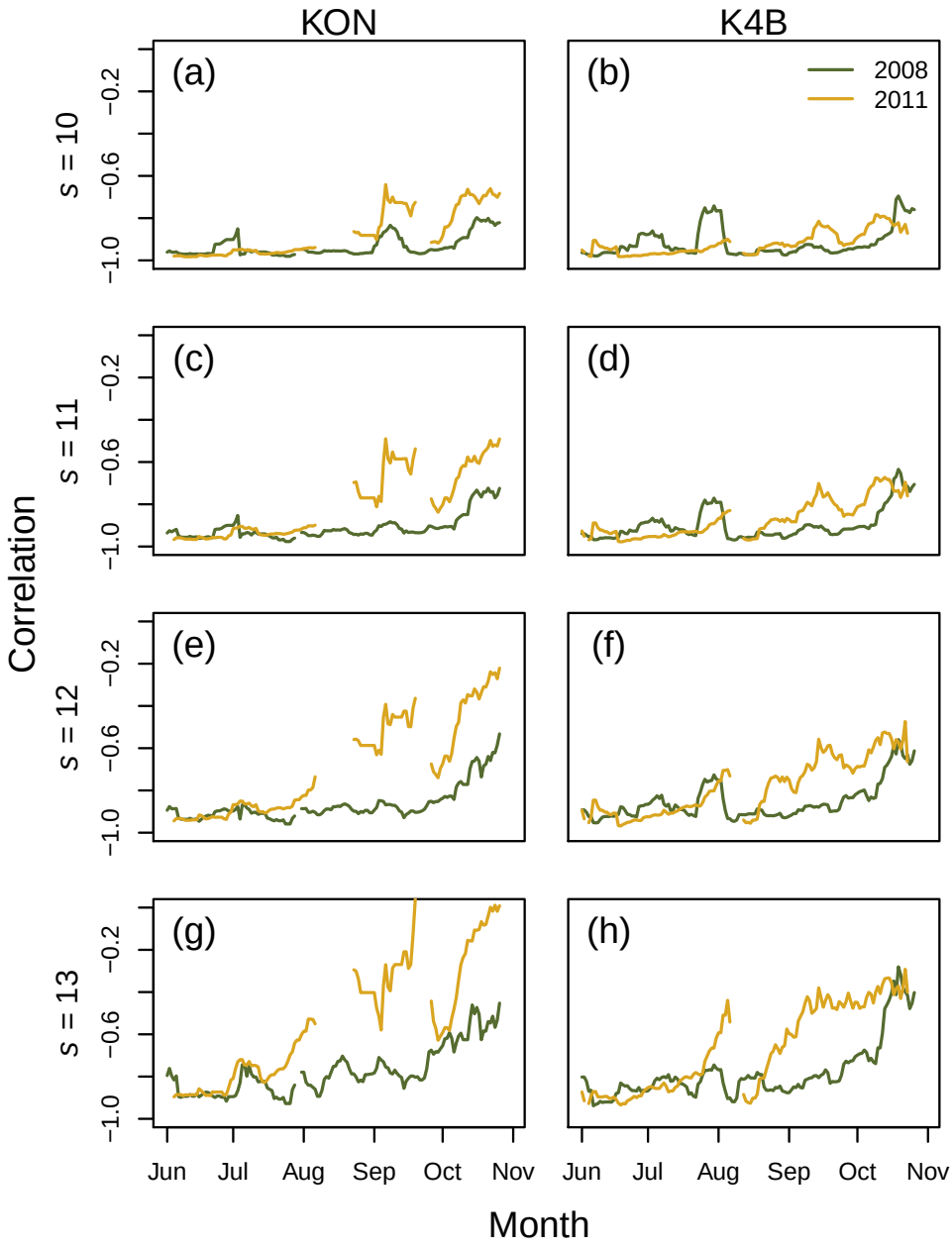

Figure 2.7: Five-day moving average of correlation of water vapor and CO_2 fluxes by wavelet scale, *s*, of 10 through 13 (corresponding to timescales of 51.2 - 409.6 s) at KON (left column) and K4B (right column) for 2008 (green) and 2011 (gold). Correlation varies significantly ($p<0.01$) between sites K4B and KON in 2011 only, at all four scales. Within sites, at KON there is a significant difference between 2011 and 2008 at all scales plotted, while K4B only varies significantly between these years at $s = 12$ and 13. Gaps in time series are indicative of series of three or more days which contained too many missing data points (>0.5%) and were therefore excluded from the analysis.

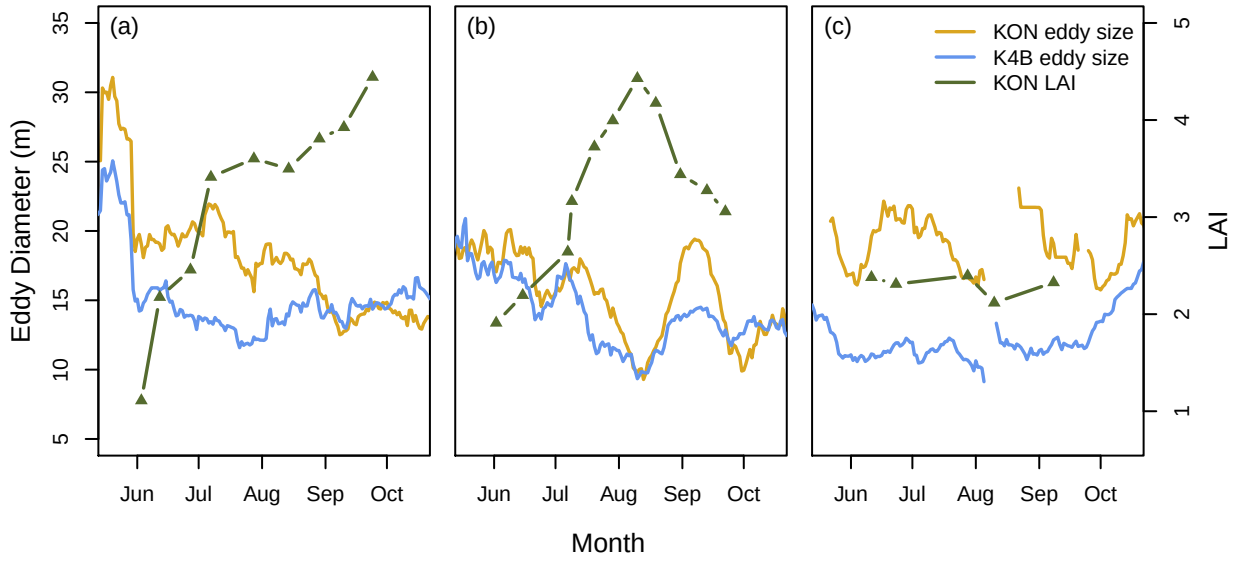

Figure 2.8: One-week moving average of eddy diameter (m) of maximum scalar transport for 2008 (left), 2009 (middle), and 2011 (right) at KON (gold) and K4B (blue). Leaf area index as measured at KON for each year is also shown (green, right axis).

negative *cq* correlation after the onset of drought conditions in 2011. This breakdown is most evident at the larger scales (*s* of 12 and 13) and particularly pronounced at the annually burned site. Based on mean wind speeds at the sites, these scales correspond to eddies of approximately 512 to 1,840 meters in diameter. A significant early seasonal breakdown with drought was not detected in correlations of the complete time series.

Differences between sites and across years in the eddy diameter of maximum contribution of net CO_2 and water vapor flux was investigated through the daily sums of WCs, which indicate the relative contribution to the overall flux of a scalar transported by eddies of each scale. The eddy size of maximum transport for *c* and *q* was very similar in both magnitude and seasonal pattern, so only *q* results are shown here. K4B had smaller average eddy diameters of maximum transport than KON across all years (Figure 8), averaging 16.4, 14.7, and 13.2 m while KON averaged 19.3, 16.9, and 20.2 m in 2008, 2009, and 2011, respectively. Peak eddy diameters were closest between sites in 2009, when both sites were burned at the beginning of the growing season. Eddy size of peak transport decreased across the growing season as canopy height and LAI increased. Overall seasonal pattern showed a strikingly inverse relationship to measured LAI.

Unfortunately, measured LAI was only available across all years of the study at KON. Difference in eddy size could be primarily due to decreases in height of the tower above the canopy as the grass height grows; however, eddy size showed an increase with decreasing LAI at the end of the growing season in 2009. Additionally, peak eddy transport size at K4B was lowest in 2011, despite having less growth time since the previous burn than in 2008. This is could be explained by the increase in fire-resistant dogwood patches over recent years. It is inferred that differences in eddy size of maximum q and c transport were primarily caused by changes in both canopy height and surface roughness in combination. The difference in eddy diameter between sites was largest during drought conditions, remaining large until October when eddy size at K4B increased. This is also indicative of an increase in eddy size and decreased effective surface roughness with lowered plant activity.

Overall, wavelet analysis shows that differences in momentum with woody encroachment was seen across small to medium scales, over eddies of an average of 4.0 to 95 m at K4B and 5.2 to 108 m at KON. These same scales transported most of the net q and c fluxes, as seen by the range of eddy diameters of maximum transport calculated from the daily sum of WC. However, a breakdown of scale-wise cq correlations from -1 occurred significantly with drought only at much larger scales, averaging approximately 512 to 1,840 m in diameter. Variance in cq correlations did increase across all scales in 2011 at KON only, corresponding to the overall changes in plant activity seen at this site with the drought.

2.4 Summary and Conclusions

This study utilizes the unique opportunity provided by closely located eddy covariance towers on prairie sites of differing levels of woody encroachment to build upon current understanding of how changes in species' composition can alter regional carbon and water budgets through alterations of productivity, WUE, source water depth, and turbulent flux dynamics. Of particular focus is how woody encroachment alters the regional impact of drought. Overall, the change in plant composition in the area with a lower burn frequency has been encroachment of shrubby plants,

including a recent sudden increase in dogwood patches at K4B, where they now make up over 50% of the land cover. Established dogwood patches are more fire resistant (Ratajczak et al., 2011), providing a positive feedback for further encroachment.

Measured carbon uptake was greater across all years at the site experiencing encroachment. This general trend was expected given the much greater NPP of Dogwood (Lett et al., 2004). CO_2 flux into the ecosystem at K4B was nearly double that at KON in 2008 and is more than triple that at KON in 2009. The difference between sites becomes most stark in 2011, when drought conditions occurred during the growing season and the annually burned grassland became a negligible sink and possibly even a source given the additional error range due to flux not measured during burning. This is in line with the results of many other studies of source/sink status of grasslands (e.g. Schwalm et al. 2010; Aires et al. 2008; Meyers 2001).

Despite the generally higher leaf-level WUE of C_4 grasses (Ehleringer & Monson, 1993) and greater proportion of C_4 plants at KON, the net seasonal WUE was greater at K4B during wet conditions. Those results support recent findings of Brunsell et al. (2014). However, during drought conditions, greater seasonal WUE was seen at grasslands not experiencing woody encroachment. During the drought, plant productivity at KON was much lower, but the site also lost far less water. Previous research has shown that woody encroachment can result in increased groundwater usage (Scott et al., 2006), and stable isotope analysis has indicated that dogwood patches pull from deeper sources of soil moisture (Nippert & Knapp, 2007a). Our results support these findings, showing evidence of depletion of deeper, stored water resources with woody encroachment as cumulative ET surpassed cumulative precipitation at K4B during drought. The access to stored moisture results in greater photosynthesis occurring during otherwise drier conditions, which results in increased NPP with decreased WUE.

How these measured changes in net fluxes and potential changes in effective surface roughness and heterogeneity are reflected in overall structure of fluxes was also investigated using MOST, quadrant-hole analysis, and wavelet decomposition. Increased surface heterogeneity and patchiness with woody encroachment was seen through a weakened applicability of MOST at K4B. This

effect overwhelmed any change in source/sink distribution with drought onset. Increased LAI and productivity coincides with increased ejections from the canopy. At both sites a slight decrease/increase in contribution of net momentum flux from sweeping/ejecting motions from the boundary layer/canopy took place over the course of the growing season. Net exchange of CO_2 and water vapor were primarily transported by ejections from the canopy.

Wavelet decomposition was used to determine dominant scales of these motions, the size of eddies involved in net exchange, and how they change with species composition and drought. Analysis shows differences in power between sites across small to medium scales, over eddies with an average diameter of 4.0 to 108 m. Using the sum of WC method, eddy sizes within this range were shown to also transport the largest portion of total CO_2 and water fluxes. Eddy diameter of maximum transport decreased seasonally in a pattern strikingly inversely related to measured grassland LAI, and was lower at K4B across all years, likely from increased LAI and effective surface roughness. A breakdown of scale-wise *cq* correlations from -1, representing a decrease in the amount of plant activity being transported at each scale, occurred significantly with drought only at much larger scales, averaging roughly 512 to 1,840 m in diameter. However, an increase in variance of *cq* correlation is seen across scales in 2011 at KON only, coinciding with decreased plant activity at this site during drought. Woody encroachment caused significant changes in power across small to medium scales, encompassing the eddies which exchange most turbulent fluxes. There was a decrease in average size of eddy transporting fluxes, but an increase in total fluxes of both CO_2 and water with woody encroachment, which coincides with the significant increase seen in the wavelet power spectrum at these small to medium scales.

Overall, results are indicative of dampened plant response to drought with woody encroachment due primarily to changes in root access. Results suggest that on a regional scale, increases in woody encroachment with human-driven land cover changes have caused increased carbon sequestration and ecosystem WUE during non-drought conditions. Given the projected increases in aridity with climate change, this would be a welcome shift. However, this study also indicates that in times of drought the benefit of woody encroachment-induced increases in WUE disappear and

greater depletion of stored groundwater may occur.

Chapter 3

Comparison of land-atmosphere coupling metrics using long-term eddy covariance measurements at heterogeneous grassland sites

3.1 Introduction

Local feedbacks between land surface conditions and precipitation can result in sustained impacts well beyond the duration of a single precipitation pulse or abnormal dry spell, which can, in turn, exacerbate or mitigate potential droughts on a regional scale. Given recent severe droughts (Wolf et al., 2016) and expected increases in drought frequency and severity both globally and regionally in the central U.S. (Dai, 2012), quantifying land-atmosphere (LA) coupling is vital to projecting consequences of forecast climate change.

Many studies have developed different methods to assess LA coupling strength (e.g. Koster et al., 2006; Santanello et al., 2009; Findell et al., 2011). Their findings indicate that coupling strength is highly variable across the United States, and depends heavily on antecedent soil conditions (Harding & Snyder, 2012a,b; Wei et al., 2013), so can be strongly affected by prior drought conditions. Grassland ecosystems in particular are considered quite sensitive to changes in precipitation amount and timing (Blair et al., 2013), and the Central Great Plains have been categorized as both a "hot spot" of strong LA coupling by some metrics (Koster et al., 2006; Christensen et al., 2007; Notaro, 2008), but also found to be relatively weakly coupled by other studies (Brunsell, 2006; Findell & Eltahir, 2003b; Findell et al., 2011). Such profound disagreement among LA coupling metrics is alarming, particularly in a region of extensive land management and agricultural

production.

Long-term near-surface flux observations by eddy covariance towers on neighboring grasslands under different management practices are used as a case study to compare LA coupling as diagnosed by a variety of metrics. Local feedback strength calculated from nine years of continuous tower observations over a variety of wet, normal, and drought conditions allow for detailed analysis of when and how coupling metrics contradict and under what conditions, if any, there is consensus. Additionally, the proximate prairie sites operate under differing managed-burn schedules, resulting in diverging species' composition and vegetation structure with rapidly increasing woody encroachment during the period of observation at one of the prairie sites. By contrasting LA coupling metrics between sites this study aims to identify how woody encroachment, a phenomenon taking place across grasslands globally (Blair et al., 2013; Saintilan & Rogers, 2014), changes LA coupling and whether metrics are more attuned to conditions at one type of vegetation structure or the other.

3.1.1 Land atmosphere coupling defined

LA coupling has been defined as "the impact of land surface states on the evolution of surface fluxes, the planetary boundary layer (PBL) and free atmosphere, including clouds and precipitation, as well as positive and negative feedback mechanisms that modulate extremes" by the Global Land-Atmosphere System Study's (GLASS) panel on Local LA Coupling (Santanello et al., 2017). This complex interaction between the land surface and atmosphere involves soil moisture, evapotranspiration (ET), surface sensible and latent heat flux partitioning, PBL evolution, and precipitation, with a full feedbacks requiring several legs of interaction between variables that cause the initial increase/decrease in a variable to eventually feedback upon itself and cause further increases/decreases.

One leg of the full LA coupling feedback - the influence of precipitation on soil moisture - is direct and easily understood. The influence of soil moisture on ET is more complex, but can be divided into three general regimes of moisture availability (Seneviratne et al., 2010). In a dry regime

soil moisture is below the threshold at which transpiration cannot take place due to low matric potentials. In wet regimes moisture is plentiful, ET is able to reach potential evapotranspiration (PET), limited only by energy availability. In the transitional regime, ET varies as a function of soil moisture availability. Although the actual relation is complex, it can be approximated within this transitional regime by a linear change in ET with soil moisture - a pattern broadly observed in models based on much more complex interactions and in Fluxnet observations (Koster et al., 2006; Seneviratne et al., 2010). However, whether an area falls into a particular regime is highly dependent on the availability of moisture in the soil for evapotranspiration, which varies with land cover properties such as the rooting depth of plants (Flato et al., 2013). Regions may switch between regimes of limitation on ET over the course of a year and may also switch regimes due to changes in land cover or extreme events such as drought (e.g. Roundy et al. (2013); Roundy & Santanello (2017); Zaitchik et al. (2013)).

A full positive (or negative) feedback loop requires a third relation - that of increased (decreased) ET to increasing (decreasing) precipitation. This relationship is more complex as ET has a large and direct impact on the energy cycle as well as the hydrological cycle. Increases in ET are an increase in energy partitioned to latent heat; in fact, ET has been shown to use more than half of the total energy absorbed by the land surface from solar radiation (Trenberth et al., 2009). Lower ET values increase sensible heating and thus increase turbulent mixing and PBL growth, while higher ET values provide the moisture needed for convective precipitation and moist static energy (Seneviratne et al., 2010). The contrasting influences of ET on convective potential is seen through studies finding enhanced convective instability over drier soils under some circumstances (Findell, 2003; Findell & Eltahir, 2003a,b; Ek & Holtslag, 2004), though most find wetter soils increasing potential precipitation to varying degrees depending on antecedent conditions (Seneviratne et al., 2010).

The strength of LA couplings is be further complicated by regional differences in climate, plant type, soil type, land management, etc. Soil types vary greatly in water holding capacity and the ease with which evaporation or transpiration can occur. Additionally, soil has a “memory" of previous

conditions, known as hysterisis (Hillel, 1998), which causes antecedent soil conditions to have an on LA coupling strength. Soil moisture also affects the color of soil, altering its albedo and influencing available energy, usually lowering with increased moisture, increasing total heating. Human management such as irrigation is another complicating factor. In the Great Plains, most of the water applied to the surface through irrigation is evaporated or transpired (Harding & Snyder, 2012a), with much of it recycled locally as precipitation (Huber et al., 2014; Wei et al., 2013). Managed prairie burns and the reduction of natural burns can have a strong impact as well by changing plant composition. Transpiration is the larger component of ET (Dirmeyer et al., 2006; Lawrence et al., 2007), so the rooting depth and water use efficiency of plant species present has a large influence on LA coupling. Theoretically, the same soil moisture conditions with different land cover and plant activity could result in very different, even opposite direction, LA coupling feedback.

3.1.2 Metrics

Early studies on LA coupling have focused on large-scale feedback between soil moisture and precipitation (Santanello et al., 2017). The most prominent one may be the Global Land Atmosphere Coupling Experiment (GLACE), which compared variance of precipitation and prescribed land cover variables in ensemble model output. The difference between test and control ensemble runs is used to determine the relative contribution of the prescribed surface variables to the generation of precipitation in a region, thus identifying "hot-spots" of strong LA coupling, which included the Central United States (Koster et al., 2006). This metric, by definition, depends on model output. So, although it is a useful metric for assessing model behavior and explaining predictability, it has no real-world equivalent and cannot be determined observationally. Numerous studies followed up on GLACE, creating and using a variety of coupling metrics in an effort to locate coupling hotspots (Santanello et al., 2017).

The most common multi-variate statistic method used to investigate interactions between variables is a simple correlation or covariance. The feedback parameter (FBP), developed by Notaro

(2008), uses lagged covariance ratios to locate hotspots of soil moisture feedback. The ratio of covariance of precipitation and soil moisture to soil moisture auto-variance is used to represent the fraction of precipitation changes attributable to variations in soil moisture. FBP and similar lagged covariance metrics have been used in several studies (e.g. Zhang et al., 2008, 2009; Zeng et al., 2010; Spennemann & Saulo, 2015). Using output from 19 climate models used in the IPCC's Fourth Assessment Report, Notaro (2008) identified the central United States, among other regions, as a statistically significant hotspot, with soil moisture influence on precipitation peaking in June/July for the region. However, the same region was not classified as a significant hotspot when FBP was calculated using precipitation from Climate Prediction Center Merged Analysis of Precipitation (CMAP) and soil moisture from the Global Land Data Assimilation System (GLDAS) (Zhang et al., 2008). Orlowsky & Seneviratne (2010) found that FBP showed large discrepancies when calculated using output from different GCMs. Additionally, they showed that apparent soil moisture – precipitation feedbacks are often just as attributable to the influence of sea surface temperatures on precipitation. A study by Sun & Wang (2012) also concluded that sea surface temperature and ocean circulations often playing a larger role in precipitation variability and that FBP usually overestimates the impact of soil moisture on local precipitation. However, the US Great Plains was identified as the sole FBP hotspot with potentially accurate feedback estimates (Sun & Wang, 2012). Since it attempts to connect soil moisture variations to precipitation, the FBP is designed to capture the totality of the LA coupling chain. However, this also means it overlooks many intermediate steps in the process and compensating errors can be hidden. Additionally, the basis of the metric in covariance means high values can hint at causation, but it is important to remember that high FBP does not necessarily mean there is a direct influence.

Many metrics have been developed that focus specifically on a single step or component of the LA coupling chain. The Priestley-Taylor Ratio (PTR), a measure of the efficiency of surface evaporation to the PBL, is one such metric. It is the coefficient in the Priestley-Taylor formulation of potential evaporation, and is generally interpreted as the ratio between actual evaporation rate and equilibrium evaporation rate (Eichinger et al., 1996). PTR accounts for the fact that entrain-

ment from the top of the PBL will dry the mixed layer, allowing more water vapor flux into the atmosphere (Betts, 1994). With no entrainment and plenty of available moisture, PTR would be expected to have a value of 1, so values above that are indicative of mixing of dry air from entrainment. Priestley & Taylor (1972) proposed that the ratio has a nearly-constant value around 1.26 over a variety of moist surfaces in equilibrium, representing a balance between surface and entrainment processes. Many studies have since generally supported that proposition, finding that PTR values range between 1.2 and 1.3 over vegetation in the absence of water stress (Raupach, 2001; Betts, 2004; van Heerwaarden et al., 2009). Higher values suggest stronger entrainment (pointing to a deeper PBL), reduced aerodynamic resistance, or increased canopy resistance, while lower values are common in water-limited conditions. Thus, PTR can be used to reveal how surface changes in canopy structure influences entrainment at the top of the boundary layer. PTR is a metric ideally suited to flux tower measurements; however, it can be difficult to separate the many noted potential causes of higher/lower PTR values.

Another branch of LA coupling diagnostics, built on work by Findell & Eltahir (2003a,b), attempts to better account for conditions throughout the atmospheric profile. The measure uses convective triggering potential (CTP) and low level humidity index (HI) to categorize LA coupling into 'regimes' based on the premise that either wet or dry soils can be more likely to trigger convective precipitation depending on the initial atmospheric state (Santanello et al., 2017). When the atmospheric profile is close to moist adiabatic lapse rate and convection could be triggered by increase in moist energy flux from the surface, the space is considered in the wet coupling regime. Coupling regime is classified as dry when the atmosphere is drier with a temperature profile closer to the dry adiabatic lapse rate where surface heating and sensible heat flux could lead to convection. When conditions lie between those two states, the regime is considered transitional. In conditions where the land surface cannot play a significant role, such as when the lower atmosphere is so dry that moisture evaporated from the surface cannot increase the boundary layer's moist static energy enough to allow for convection, the coupling regime is classified as atmospherically-controlled because precipitation would require large-scale atmospheric advection.

Findell & Eltahir (2003b) used radiosonde data to map which regime dominates local atmospheric conditions across the U.S. The Great Plains are classified as a transitional region in the CTP-HI framework, with neither wet nor dry soil consistently favored for convection. Ferguson & Wood (2011) developed a methodology to derive dataset-specific thresholds of the CTP-HI classification of convective regime and derived the metric globally using satellite data sources in order to make up for the lack of observationally-based data for evaluating model based estimates of LA coupling strength. Results also did not show a consistent wet or dry advantage for the Central U.S. region.

Roundy et al. (2013) built upon this diagnostic by developing a metric that can calculate daily wet- or dry- soil advantage and which takes soil moisture conditions into account. The CTP-HI space is divided into the categories of coupling regime based both on the potential for moisture to drive precipitation and on the local statistics of soil moisture associated with that region of CTP-HI space (Roundy et al., 2013, 2014). Because it is based on local statistics, the classification is not standardized across regions, but is calibrated to the location and period over which it is computed. A time-series of dominant coupling regime at a particular location is then turned into the coupling drought index (CDI) over a period of days by calculating the difference in number of dry vs wet coupling days divided by the total number of days. This way persistent wet/dry states are indicated by higher values of the metric. Calculation of CDI requires a great deal of information about the atmospheric profile and soil moisture, which can be difficult to consistently observe at a location, so has generally been derived from a combination of in situ data and reanalysis products. Recently, however, Roundy & Santanello (2017) derived CDI solely from an observational platform by using AIRS satellite profiles.

3.1.3 Motivation

As shown above, there is frequent disagreement between LA coupling metrics, notably in diagnosis of the Central US region as a “hotspot” or not. Analyzing the accuracy of LA coupling metrics can be difficult as many are based on different portions of the LA coupling chain and use different scales or types of input, therefore are not always directly comparable. Basing an assessment on a

single variable, such as accuracy in predicting drought or precipitation, does not necessarily reveal a causal relationship and runs the risk of overestimating the strength of a metric as confounding errors may mitigate each other. In order to investigate the sensitivity of metrics more fully, a methodology developed for model intercomparison by Santanello et al. (2009, 2011) based on Betts (1992)'s mixing diagrams (MD) is used.

MD are plots of the diurnal evolution of near-surface specific humidity (q) and potential temperature (θ) in energy space. Much can be deduced about the boundary layer evolution from these diagrams, including estimates of flux from entrainment at the top of the PBL. This can then be used to quantify diagnostics including the Bowen ratio of surface and entrainment fluxes, and the proportion of heat input from entrainment to that from the surface. The strength of this method is its easy to interpret visualization of flux development over the day and quantification of important components in many steps of a complete LA feedback loop (Santanello et al., 2015). In this study, MD are used to investigate whether the metrics are actually able to separate out distinct diurnal surface flux conditions and capture meaningful differences in surface effects on the PBL growth and thus potential precipitation conditions.

Another potential concern with LA coupling metrics is their usefulness to assess complex conditions or predict behavior beyond what other, more easily observed or calculated metrics could do. If a metric fairs no better than, for instance, a simple soil moisture assessment at predicting surface flux partitioning, PBL growth, and precipitation likelihood, then it provides no added value and its usefulness is questionable. One way to assess this is to look at the sensitivity of coupling metrics to a variety of meteorological variables or environmental patterns. Self-Organizing Maps (SOM) are an ideal tool for identifying significant meteorological states that occur at the study site. SOM convert complex, nonlinear statistical relationships between high-dimensional input data into low-dimensional geometric relationships for easy interpretation of patterns (Kohonen, 1995). An advantage of SOM is that the process is unsupervised, requiring no target vectors, consequently results are not influenced by user assumptions (Kangas & Kohonen, 1996). SOM can be used to identify a comprehensive range of meteorological states at the study site, which can then be used to

identify what more complex patterns of environmental conditions, if any, the metrics are sensitive to.

Through comparison of common coupling metrics over nine years of high frequency flux observation at two prairie sites with differing management but very similar large-scale climate forcings due to proximity, this study investigates several questions:

- Are these sites, which are located in the Central US, “hotspots" of particularly strong LA coupling? Do the discrepancies between metrics in this area remain when calculated over the field-scale study sites?
- Does land management strategy and the resultant differences in grassland vegetation structure alone significantly alter LA coupling between these sites? And, if so, how does this heterogeneity affect the accuracy or ability of the LA metrics?
- How much do simpler classifications, such as categorization by soil moisture or precipitation deviations, explain coupling strength? What other meteorological states are influential to the coupling metrics?

3.2 Methods

3.2.1 Site description

This study utilizes two continuously operating eddy covariance towers at prairie sites in Kansas with diverse management practices. The towers located less than a mile apart in the Konza Prairie Long Term Ecological Research (LTER) station - a 3,487 hectare native tall-grass prairie in north-eastern Kansas, USA (39.08°N, 96.56°W). The first tower (KON) is on an annually-burned (since 1978) watershed in an upland topographic area (Bremer & Ham, 2010). The second tower (KFB) is in a lowland watershed managed with prescribed burns every four years since 1975 (Brunsell et al., 2014). Managed burns are generally carried out in late April. Over the span this study KFB was burned in 2009, and 2013, and KON was burned each year. The native prairie sites are

dominated by four perennial C_4 grass species: big bluestem (*Andropogon gerardii*), little bluestem (*Schizachyrium scoparium*), switchgrass (*Panicum virgatum*), and indiangrass (*Sorghastrum nutans*). However, the less-frequently burned KFB has seen an explosion of dogwood (*Cornus drummondii*) during the years of observation, with fractional coverage of shrub now at over 50%.

The sites are in a mesic grassland with mean annual precipitation of 847 $\pm$171 mm. The study period spans from 2008 through 2016, which contain a wide variety of moisture conditions including abnormally cool, moist years with a high of 1153mm of precipitation in 2008, and years with a significant droughts, with as little as 565mm of precipitation falling in 2012. The proximity of the two sites means they receive nearly identical amounts and timing of precipitation, ensuring that differences in land-atmosphere interactions are driven primarily by management and the resultant differences in vegetative composition.

Eddy covariance towers collected data 3.0 m above the surface at 20 Hz. Temperature and three orthogonal components of wind velocity were collected using a Campbell Scientific CSAT-3 triaxial sonic anemometer and water vapor and carbon dioxide concentrations were collected with a Li-Cor 7500 open-path gas analyzer. Latent (LE) and sensible heat (H) fluxes were computed using the eddy covariance method (Baldocchi et al., 2001). In addition, net radiation, soil moisture, and precipitation measurements were collected at the sites. Observations were collected and stored using a Campbell Scientific CR 3000 Datalogger. Further information on site instrumentation and processing can be found in Brunsell et al. (2014). Data were processed to half-hourly averages following AmeriFlux standards and is available on the AmeriFlux site (http://ameriflux.lbl.gov/).

3.2.2 Coupling Metrics

A variety of detailed metrics of land-atmosphere coupling strength are calculated using data from eddy covariance towers, remote sensing, and reanalysis. Wherever possible, tower observations alone are used.

3.2.2.1 Feedback parameter

Feedback parameter (FBP) is a simple statistical method to estimate the feedback between a large-scale, slowly changing variable (soil moisture, in this case) acting on a shorter-time-scale variable (here, precipitation) (Frankignoul & Hasselmann, 1977). Precipitation (P) at a time $t + dt_a$ is assumed to be composed of contributions from soil moisture (S) at time t and from atmospheric internal variability, or noise, (N) at $t + dt_a$, with t_a being the atmospheric response time. Expressed as a function, this is: $P(t + dt_a) = \lambda S(t) + N(t + dt_a)$, where λ is the FBP and represents the sensitivity of precipitation to soil moisture. To solve for λ, the covariance with soil moisture at a time t - τ is taken on both sides:

$$\langle S(t-\tau)P(t+dt_a)\rangle = \lambda \langle S(t-\tau)S(t)\rangle + \langle S(t-\tau)N(t+dt_a)\rangle \tag{3.1}$$

So long as τ, the lead time for soil moisture influence on precipitation, is longer than t_a, which is typically less than a week, the last term of the equation will equal 0 because soil moisture leading that response time will not have an impact on later noise, and atmospheric noise cannot influence earlier soil moisture. If τ is much longer than the atmospheric response time, the dt_a term can be neglected. Rearranging yields:

$$\lambda = \frac{\langle S(t-\tau)S(t)\rangle}{\langle S(t-\tau)P(t)\rangle}. \tag{3.2}$$

Thus, FBP is the ratio of lagged covariance between soil moisture and precipitation to the lagged auto-covariance of soil moisture. It represents the average response of precipitation to changes in soil moisture over the window calculated. Input values are seasonally detrended using a sinusoidal best fit on annual average data at both sites to ensure that the regular seasonal patterns of precipitation and soil moisture do not dominate the parameter. In order to stay consistent with the assumptions used in the above derivation, but also facilitate comparison with metrics on much shorter timescales, λ is calculated daily, using a moving window with a τ of 4 weeks.

3.2.2.2 Priestley-Taylor Ratio

Daily PTR values are calculated at each site from EC tower flux observations averaged from 7am-7pm, based on Dirmeyer et al. (2013) and Betts (2004) as:

$$\text{PTR} = EF\left(\frac{1+\varepsilon}{\varepsilon}\right), \varepsilon = \frac{\lambda}{C_p}\frac{dq}{dT}\Big|_{T_{LCL}}, \tag{3.3}$$

where EF is the evaporative fraction, calculated as $LE/(H+LE)$, using latent heat (LE) and sensible heat (H) fluxes as measured by the towers. ε, the thermodynamic coefficient, is calculated using change in saturation mixing ratio with temperature (T) at the lifted condensation level (LCL) height of $z_{LCL} = (T_{tower} - T_{d,tower})/(\Gamma_{dry} - \Gamma_{dew})$ with standard lapse rates, Γ.

3.2.2.3 Coupling Drought Index

The coupling drought index (CDI) was developed by Roundy et al. (2013) based on the persistence of land-atmosphere coupling state. Coupling states are classified as dry, wet, transitional, or atmospherically controlled coupling regime, defined in Findell & Eltahir (2003a)'s joint probability space of convective triggering potential (CTP) and low-level humidity index (HI), and soil moisture conditions. CTP, HI, and soil moisture are derived from Atmospheric Infrared Sounder (AIRS) data. The CTP-HI space is divided into the categories of coupling regime based on the potential for moisture to drive precipitation, and on the local statistics of soil moisture identified with that region of CTP-HI space (Roundy et al., 2013, 2014). More detailed description of the methodology and specific parameters defining each coupling regime can be found in Roundy et al. (2013).

CDI is calculated over a period of time as the difference in number of dry and wet coupling days divided by the total number of days in the window, resulting in a CDI value between -1 (for every day of the period in wet coupling regime) and +1 (dry coupling regime over the entire period). As a result of the scale of input data and proximity of KON and KFB, the study sites are in the same grid cell and thus are always classified as being in the same coupling regime

and share identical CDI values. Climatological means are calculated by assigning each coupling classification an appropriate value: -1 for wet coupling, 1 for dry coupling, and 0 for transitional or atmospherically-controlled, and averaging over 30 years. The deviation of a 7-day moving window of CDI from the daily mean is then used to quantify unusually dry or wet coupling conditions at the sites.

3.2.3 Analysis tools

3.2.3.1 Mixing diagrams

MD are plots of the diurnal evolution of near-surface specific humidity (q) and potential temperature (θ) in energy space (Lq vs $C_p\theta$, with L, the latent heat of vaporization and C_p, the specific heat). MD of average diurnal development (from 7am to 7pm) are plotted for drought and normal summers and for a variety of conditions as defined by each metric at each site.

Estimates of flux from the top of the PBL can be deduced from these diagrams using vector decomposition. The total change in Lq and $C_p\theta$ over the plotted period (from t_i to t_f) is broken down by vector decomposition into vectors representing the fluxes of heat and moisture from the land surface and from the atmosphere. Assuming a well-mixed boundary layer, the magnitude of surface vector component in the y (heat) and x (moisture) direction are calculated as:

$$C_p\Delta\theta = \frac{\overline{H_{sfc}}\Delta t}{\rho_m \overline{h_{PBL}}} \quad \text{and} \quad L\Delta q = \frac{\overline{LE_{sfc}}\Delta t}{\rho_m \overline{h_{PBL}}}, \tag{3.4}$$

using the EC tower measured surface sensible and latent heat fluxes (H_{sfc}, LE_{sfc}, respectively) averaged over the time period plotted on the mixing diagram (dt), density in the mixed layer (ρ_m), and the mean height of the PBL (h_{PBL}) over dt. The magnitude of atmospheric response vector can then be calculated by the residual between Lq and $C_p\theta$ at t_i plus surface flux vector and Lq and $C_p\theta$ at t_f. From the component vectors, surface and atmospheric Bowen ratios are calculated as $\beta_{sfc} = H_{sfc}/LE_{sfc}$ and $\beta_{atm} = H_{sfc}/LE_{sfc}$, respectively, and the proportion of sensible and latent heat flux from the atmosphere to that from the surface are calculated as $A_H = H_{atm}/H_{sfc}$ and A_{LE}

= LE_{atm}/LE_{sfc}. These are useful diagnostics of the surface – PBL coupling and are included in the MD in this study.

The atmospheric fluxes and associated ratios are designed to be indicative of entrainment from the top of the PBL, but are referred to as atmospheric response because they also include the influence of horizontal advection on fluxes and errors inherent in using 3 m EC tower measurements of temperature and humidity in lieu of mean values over the mixed layer (Santanello et al., 2013). Some inaccuracy may also be introduced by estimation of mean boundary layer height. Mean boundary layer height over the period of the MD is required for the vector decomposition as it is used to represent the volume by which the fluxes are scaled; unfortunately, PBL height is difficult to measure and LCL-based estimates are not very accurate. For this study the mean of 12pm and 6pm boundary layer heights from the European Centre for Medium-Range Weather Forecasts (ECMWF) ERA-Interim reanalysis product is used (Dee et al., 2011). Atmospheric and surface flux components are included in the MD of each coupling metric at each site. These are used to investigate whether the metrics are actually able to separate out distinct diurnal surface flux conditions and capture meaningful differences in surface effects on the PBL growth and thus potential precipitation conditions.

3.2.3.2 Self-organizing maps

SOM convert complex, nonlinear statistical relationships between high-dimensional input data into low-dimensional geometric relationships for easy visualization and interpretation of patterns (Kohonen, 1995). Initially, the SOM function defines a random distribution of nodes, defined by weighting coefficients of the input variables. SOM attempts to find nodes that are individually representative of nearby observations, and which together span the multi-dimensional distribution of the input dataset. The weighting functions are tested and adjusted iteratively to minimize the distance, usually Euclidean, from each node's weighting function to the samples represented by that node. Eventually, a minimum is reached and further iterations cannot continue to reduce the distances. Even though the measured distance between data and weighting functions is linear,

the iterative training process allows SOM to account for non-linear data distributions. For further details on the SOM process and uses in climatology, see (Hewitson & Crane, 2002).

SOM are used to identify a comprehensive range of distinct environmental states that occur at the sites during the growing seasons studied. A broad set of meteorological variables that are not directly used in the calculation of coupling metrics are selected to train the maps. Scaled, seasonally-detrended daily observations of net radiation (Rn), 3m air temperature (T_a), 3m horizontal wind speed (u), friction velocity (u_*), vapor pressure deficit (VPD), and length of time since the last precipitation event over 1mm were used as input. As the SOM process is unsupervised, nothing must be assumed about the resultant clusters of these input variables, and the only user-input SOM results are sensitive to are the selected shape and size of the grid of nodes. In this study, nodes were organized in a hexagonal grids to maximize the number of immediate neighbors of each node. To minimize the influence of user-selected grid size, a variety of sizes were tested to find the largest size that did not result in any nodes representing very few (taken to be less than 10) days. This was done to ensure the comprehensive range of meteorological states was covered without dividing the data into groups so small and specific that they no longer contain useful information about similarities among data. Hierarchical clustering was then used to group closely related nodes that described similar environmental conditions at KFB and KON, resulting in 9 SOM classifications that were then arranged in order of increasing T_a. The distribution of coupling strength within and between SOM categories is calculated for each metric.

3.3 Results

The climatological mean precipitation at Konza Headquarters is 847 $\pm$171 mm y^{-1}. The study period (2008 - 2016) covers a wide variety of precipitation conditions, visible in Figure 3.1, including the severe drought of 2012, during which the sites only received 565 mm of precipitation. 2014 and 2011 also experienced long periods of drought during the growing season, though fall and winter precipitation brought the annual precipitation totals (699 and 814 mm) to within the normal range (676 – 1018 mm). However, when considering the growing season of April through October

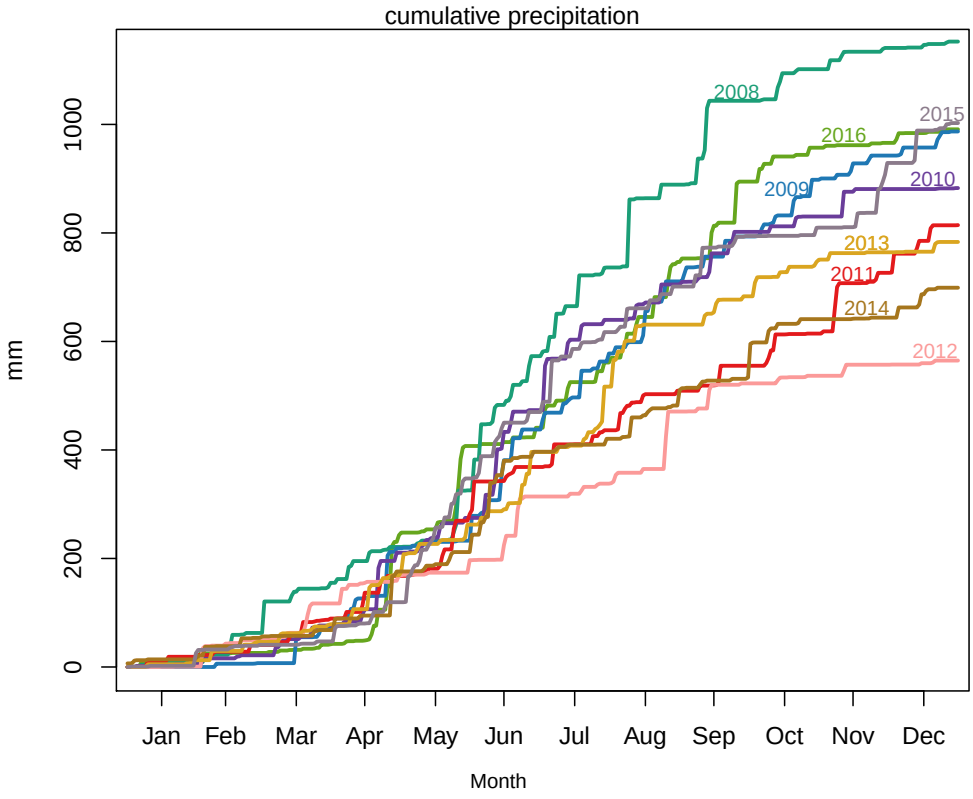

Figure 3.1: Cumulative annual precipitation (in mm) observed at Konza LTER headquarters for 2008 through 2016.

alone, the climatological mean precipitation at Konza is 682 $\pm$160 mm and 2011 and 2014 both fall below the normal range with 466 and 465 mm of precipitation, respectively. The sites received only 406 mm of precipitation during the growing season of 2012. The study period also includes the unusually wet years of 2008 and 2016, which received 889 and 852 mm of precipitation during the growing seasons alone. The rest of the study years fall within the normal range of precipitation for the region.

Daily FBP, PTR, and CDI are calculated at both sites over the growing seasons of the study period. The mean FBP for each site is very small (-0.09 at KON and 0.05 at KFB), with no significant difference between sites and no seasonal pattern aside from higher variance in the summer than winter. Figure 3.2 shows that PTR has a clear seasonal trend, typically increasing rapidly in the spring and peaking in July, with mean July PTR at KFB ranging from 1.27 in 2008 to 1.0 in 2011 and 2012. KON reaches similar, though slightly lower peak monthly PTR values (1.25 and 1.06

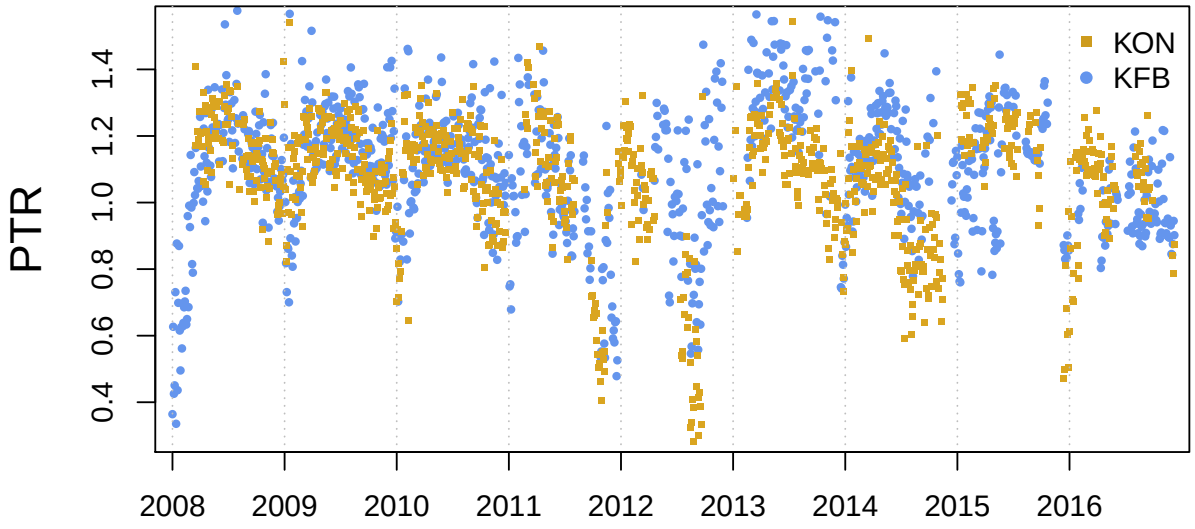

Figure 3.2: Timeseries of daily Priestley-Taylor Ratio at KON (gold) and KFB (blue) over the growing seasons (April 1 - October 31) of 2008 through 2016.

in July of 2008 and 2011). PTR typically then begins to decline in the early fall. However, during the droughts of 2012 and 2014 PTR remains steady at KFB throughout the fall, with higher than average September means of 1.12 and 1.28, respectively. Meanwhile, PTR precipitously declines in similar conditions at KON, to 0.62, 0.58, and 0.81 by September in 2011, 2012, and 2014, respectively. Overall, PTR at each site is very similar for the first four years of observation, differing by less than 0.03 on average in 2008, 2009, 2010, and 2011. The following year, during the severe drought of 2012, PTR sharply declines at KON. After this, the normal seasonal pattern returns, but the sites remain slightly separate, with KFB having 0.2 higher PTR on average for the next 2 years, before returning to similar mean values in 2015 and 2016.

Figure 3.3 shows the JJA average CDI over the central United States for two drought years (2011 and 2012) and a normal year (2013) and an abnormally wet year (2015). Konza LTER sites (KON and KFB) share the same daily classification due to their proximity and the pixel size of MERRA input data. During the years with summer drought, CDI shows enduring dry coupling conditions, averaging between + 0.5 and 1 throughout the area in 2011 and 2012. 2013 and 2015 have a much lower, though still positive, CDI, indicating dry coupling is still more frequent than

wet coupling for these summers. Annual mean CDI in the grid cell containing Konza LTERt is only -0.08, indicating no clear dominance of wet or dry coupling conditions. However, there is a strong seasonal pattern, as shown in Figure 3.4. CDI averages -0.31 the winter months (DJF), increases during the spring and summer, and peaks at 0.46 in late July. An example time series of CDI in the year of study that received the most precipitation (2008) shows more frequent periods of wet coupling, particularly strongly in August and September. A year with persistent drought conditions (2012) shows periods of more resilient dry coupling, but it not consistently and, as the region already favors dry coupling in summer, the deviations from mean are not strong, averaging only 0.07 higher than normal in JJA of 2012.

Mixing diagrams are used to visualize in energy space the diurnal evolution of surface fluxes during different coupling regimes as classified by each of the three metrics calculated and, for comparison, by a straightforward classification of drought and non-drought summers. Mean 3m potential temperature and humidity as measured by the eddy covariance towers in half-hourly timesteps from 7am to 7pm at KON and KFB for all metrics are shown in Figure 3.5. Total diurnal change is decomposed into vector components of surface and atmospheric fluxes and plotted as dashed lines, the slope of which correspond to the Bowen ratio of that component. Note that β_{atm} values are negative because the atmospheric response vector is largely made up of entrainment, which is very warm and dry, resulting in negative latent heat fluxes.

For the simple drought classification (Figure 3.5a) observations are averaged over the entire summer (June, July, and August) for two summers during which a significant drought occurred (2011, 2012) and for two summers with unusually high precipitation levels (2008, 2009). Notably, near surface near-surface mean humidity conditions are similar in wet summer at KON and both cases at KFB, with 31.1/31.2 kJkg^{-1} Lq at KON/KFB in wet summers and 31.9 kJkg^{-1} Lq at KFB in drought summers. Mean $C_p\theta$ is also relatively close in these cases, averaging 299 kJkg^{-1} at KON in wet summers, and 300/302 kJkg^{-1} at KFB in wet/dry. At KON, conditions are much drier on average during drought summers (23.4 kJkg^{-1}), though $C_p\theta$ remains similar at 299 kJkg^{-1}, and a similar pattern of drying throughout the day is visible at KON for both drought and wetter

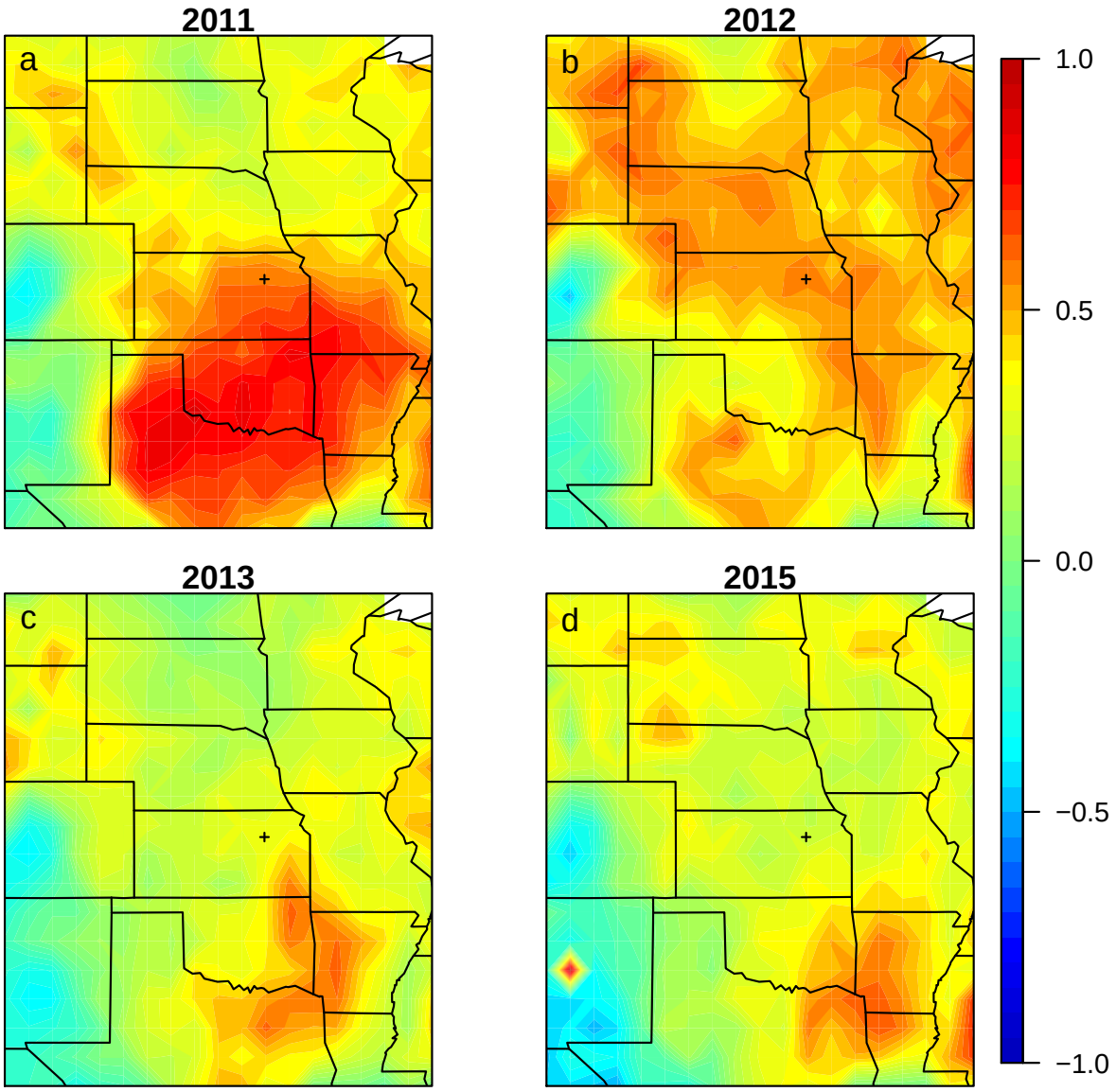

Figure 3.3: Mean June, July, and August CDI over the central United States for select years of study, including two summers with drought, 2011 (a) and 2012 (b), and two summers, 2013 (c) and 2015 (d), with normal and high summer precipitation, respectively. Konza LTER location is marked with +.

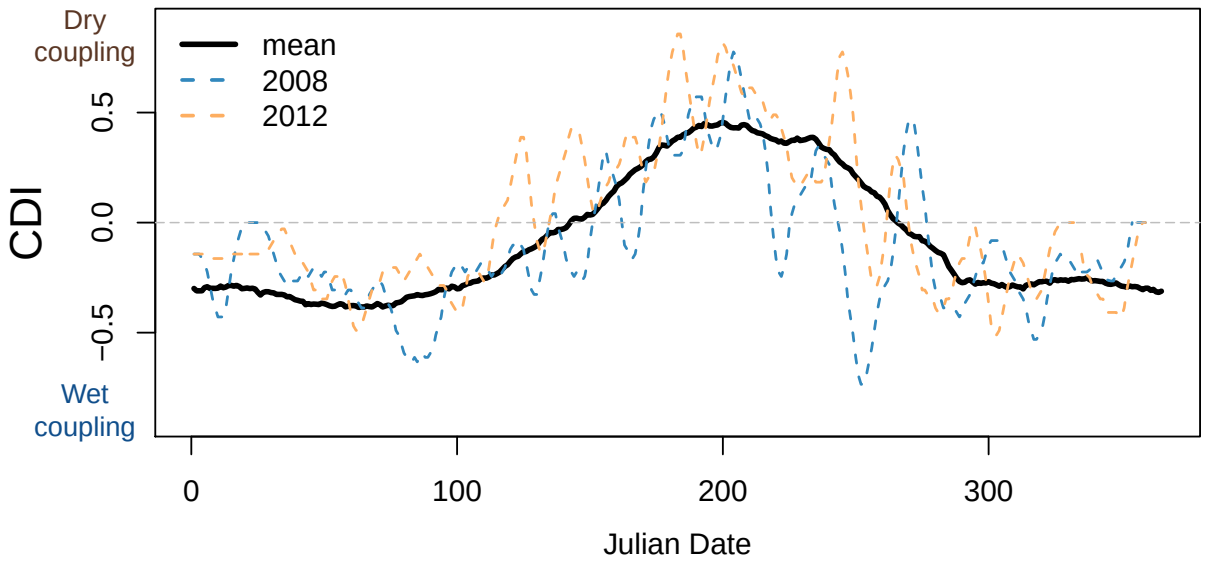

Figure 3.4: Time series of 30-year average daily CDI at the study site (black), overlain with 7-day CDI in the years with highest (2008) and lowest (2012) precipitation in blue and orange dashed lines, respectively.

summers. KFB, also displays a similar diurnal growth between drought and wet summers, with increases in q and θ throughout the day. β_{sfc} is the same (0.23) at both sites during wet summers. With drought, the Bowen ratio changes less at KFB (to 0.32) than at KON (to 0.58). However, the atmospheric response vector is much different at KFB during drought summers, bringing in far more sensible heating with a slope (β_{atm}) of -8.63. Classification by the highest and lowest 10^{th} percentiles of near-surface soil moisture measurements has very similar results (plot not included), with KFB behaving similarly at either soil moisture level, and KON responding to low soil moisture conditions through a large increase in β_{sfc} (from 0.21 to 0.70) and daytime heating and drying.

Mixing diagrams of highest and lowest 10^{th} percentile of PTR (Figure 3.5b) have a large separation of β_{sfc} by definition, as PTR incorporates evaporative fraction directly into its calculation, which is closely related to Bowen ratio. β_{sfc} varies from 0.09 to 1.05 at high and low PTR at KFB and from 0.11 to 1.23 at KON, illustrating the high latent heat fluxes in high PTR conditions. This also corresponds to higher near-surface humidity conditions, with a daily mean of 29.2 and 27.6 kJkg^{-1} at KON and KFB, respectively, compared to the much drier means of 21.8 and 21.7

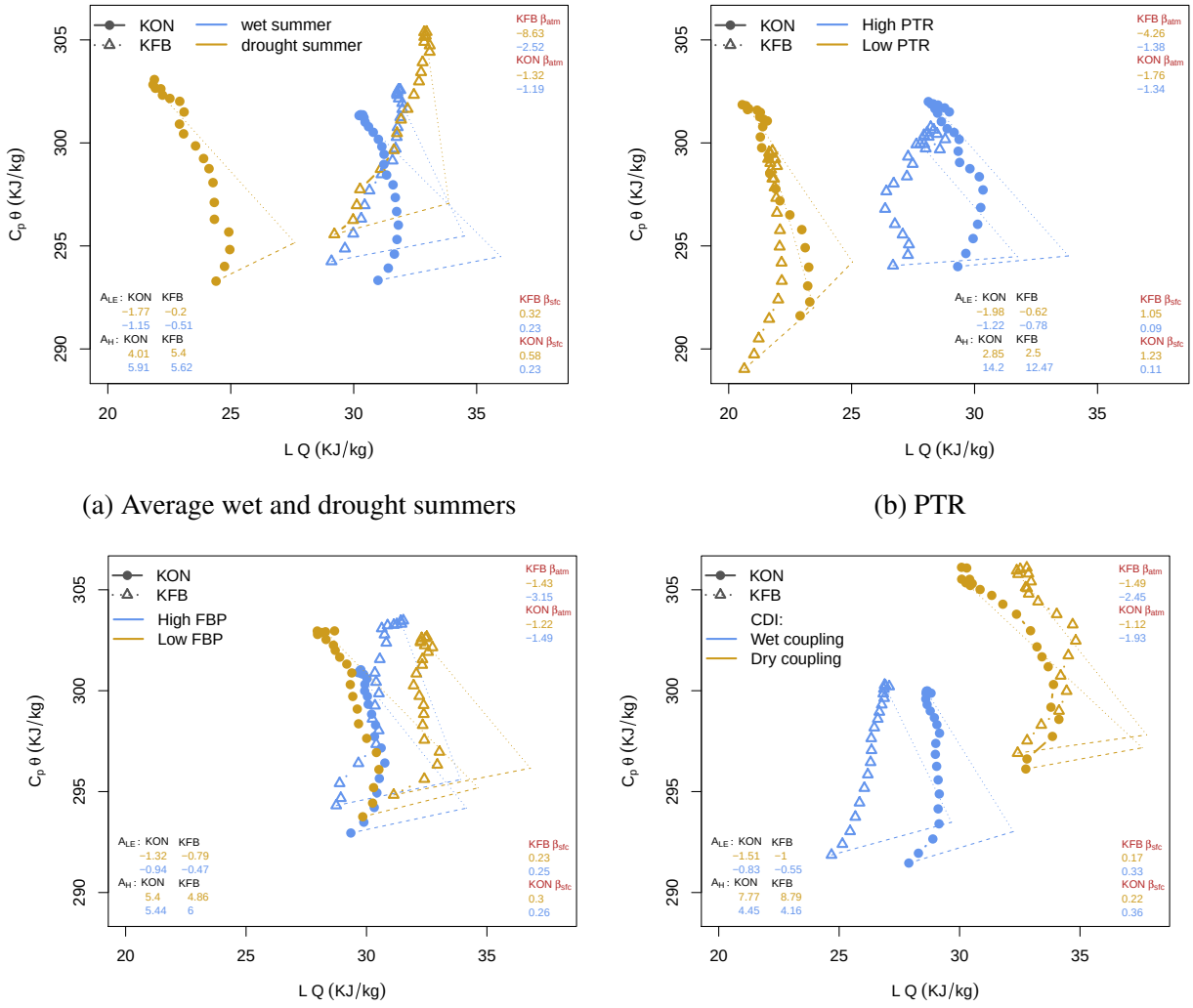

(a) Average wet and drought summers

(b) PTR

(c) FBP

(d) CDI

Figure 3.5: Mixing diagrams of 2008 - 2016 growing season mean diurnal latent and sensible heat fluxes at KON (circles) and KFB (triangles) for (a) two wet (blue) and drought (gold) years, (b) top (blue) and bottom (gold) 10^{th} percentile of PTR values, (c) top (blue) and bottom (gold) 10^{th} percentile of PTR, and (d) lowest (blue) and highest (gold) 10^{th} percentile of deviations from climatological mean CDI. Total daily flux are decomposed into surface and atmospheric component vectors, shown in dashed and dotted lines, respectively. Also included are the surface (β_{sfc}) and atmospheric (β_{atm}) Bowen ratios, and ratios of sensible ($A_H = H_{atm}/H_{sfc}$) and latent ($A_{LE} = LE_{atm}/LE_{sfc}$) heat fluxes.

kJkg^{-1} for low PTR. There is little difference in mean $C_p\theta$ between any of the four conditions, though the amount of sensible heating over the day is much higher for low PTR than for high (10.6/10.2 vs 6.7/8.0 kJkg^{-1} at KFB/KON). When PTR is high the vast majority of that sensible heat flux is from the atmospheric response vector, at a ratio (A_H) of 14.2 and 12.5 times that of surface sensible heating at KON and KFB, respectively.

Of the metrics, FBP has the least differentiation in θ, q, and β_{sfc} (Figure 3.5c). $C_p\theta$ is approximately the same at both sites, averaging between 298.3 and 300.2 kJkg^{-1} for all conditions. Mean daily Lq is between 29.8 to 30.0 kJkg^{-1} for all conditions except low FBP at KFB. Indeed, the only notable features of the MD of FBP categorizations is how similar conditions are during both high and low FBP at KON, and that the highest 90^{th} percentile of FBP at KFB corresponds to conditions similar to those at KON. The surface flux component is particularly similar between KON and KFB for high FBP, with β_{sfc} of 0.26 and 0.25 and magnitude of 5.2 and 5.7, respectively.

Wet and dry coupling CDI values are classified using the lowest and highest 10^{th} percentile of the deviations from the daily mean CDI. Diurnal co-evolution of q and θ do show distinctly different patterns for high and low CDI of growth for each site (Figure 3.5d). KFB has steadily increasing humidity and potential temperature during wet coupling, resulting in total daytime increases in $C_p\theta$ and Lq of 8.4 and 2.2 kJkg^{-1}. Wet coupling at KON also has increases in both $C_p\theta$ and Lq, totaling 8.5 and 0.8 kJkg^{-1} over the course of the day. Latent heat is not as steadily increasing at KON as at KFB, but does not show any significant periods of drying. During dry coupling at KFB there are morning increases in humidity followed by afternoon drying that results in very little total change in Lq (-0.02 kJkg^{-1}) while changes in $C_p\theta$ remain similar (8.8 kJkg^{-1}). Dry coupling at KON experiences a very similar diurnal change, but with stronger afternoon drying resulting in larger total changes of -2.5 and 9.2 kJkg^{-1} in Lq and $C_p\theta$. Counter to expectations, β_{sfc} is higher during wet coupling (0.36 and 0.33 at KON and KFB) than during dry coupling (0.22 and 0.17 at KON and KFB), corresponding to greater surface latent heat fluxes during dry coupling. Therefore, the consistent drying seen during dry coupling and increasing humidity during wet coupling must be generated by the atmospheric response vector. During wet coupling,

there is more less latent heat flux coming from the atmosphere than from the surface (A_{LE} of -0.83 and -0.55), while during dry coupling the atmospheric latent heat flux at least equals that of the surface (A_{LE} of -1.51 and -1.00).

The SOM technique is used for classification and pattern recognition for a range of meteorological variables not directly used in calculation of the coupling metrics. Resultant SOM classes are arranged in order of increasing VPD at KON. Distribution of input variables within each SOM class is shown in Figure 3.6. Some deviations are seen, such as higher wind speeds at KON than KFB (Figure 3.6d), but this is an expected result of wind speeds at KON averaging 1.5 ms^{-1} faster than at KFB. As long as any deviations within SOM classes are consistent with characteristic differences between sites, the SOM states should still be comparable. To determine if this is the case, Kolmogorov-Smirnov two sample testing is used to compare the distributions of variables within each class between sites. Conditions generally match up well between sites. Only the distribution of wind speed in SOM classes 1 and 2 and u_* for SOM classes 3 and 4 differ significantly. Coupling metrics are calculated for each SOM class to determine if the metrics are sensitive to any of the range of meteorological patterns identified.

FBP is highly variable and does not differ in a statistically significant way across any of the SOM classes or between sites within any class (Figure 3.7). PTR does change with SOM class, generally decreasing with increasing class from highs of 1.13 in class 1 at KON and 1.19 in class 2 at KFB to lows of 0.97 and 1.04, respectively, in class 9 (Figure 3.9). The changes in PTR are statistically significant for several classes at each site (1, 2, and 7 at KON; 2, 6, and 8 at KFB) and between sites for classes 2, 4, 7, and 8. These classes that differ between sites for PTR are the four classes with the lowest u (Figure 3.6d) and u_* (Figure 3.6e) of the SOM classes. Other conditions within the classes vary, from cool temperatures, low VPD, and low radiation in class 2, to high temperatures, high VPD, and high net radiation in class 8. In each of these classes, PTR is higher at KFB than at KON by around 0.08. CDI also produces significant differences between many of the SOM classes (6 of the 9 classes for KON, 5 of 9 for KFB), showing a generally increasing trend with increasing SOM class (Figure 3.8), from a low of 0.00 and 0.03 in class 1 to a high of

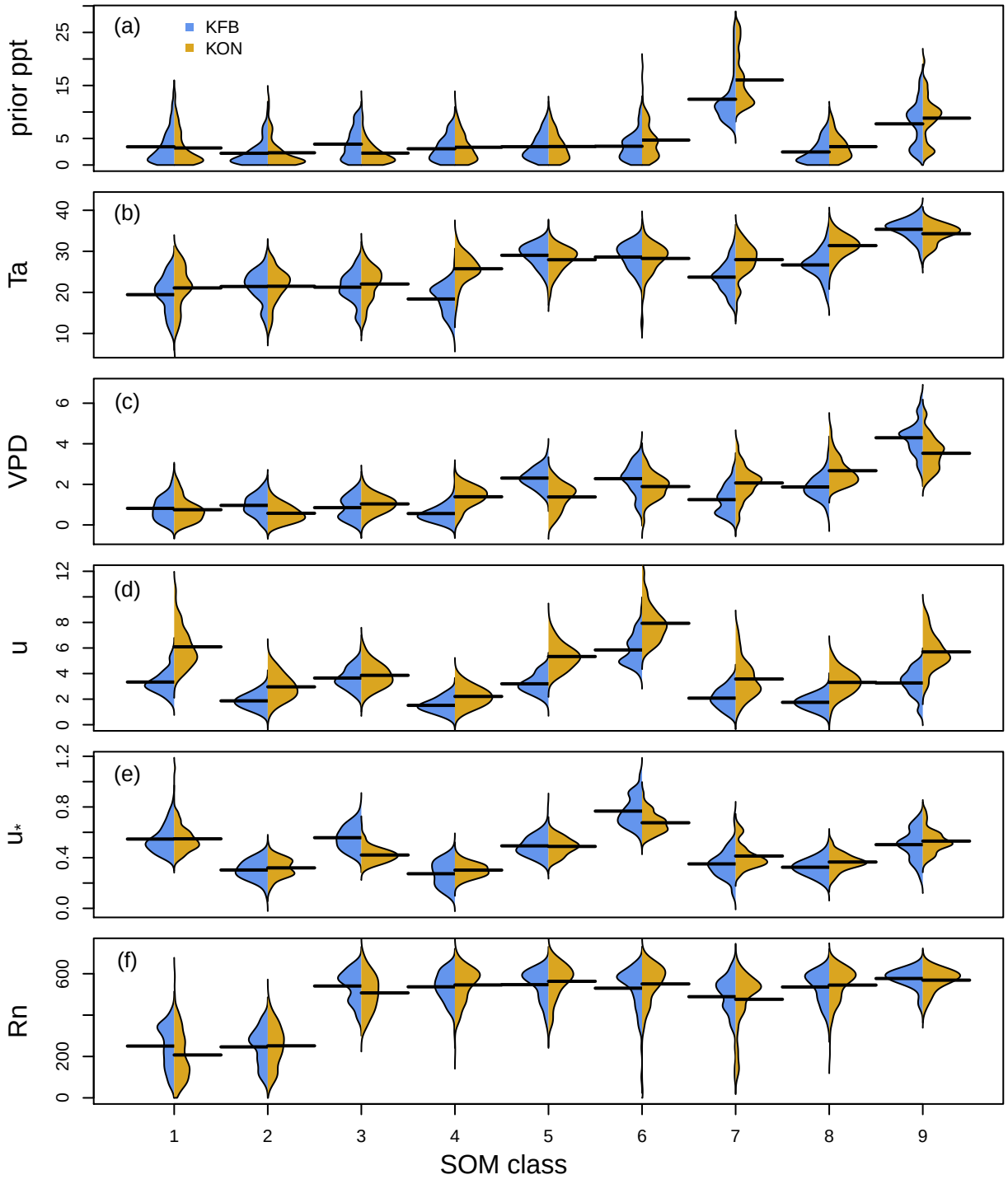

Figure 3.6: Distribution within each SOM classification of (a) days since last precipitation event, (b) air temperature (°C), (c) vapor pressure deficit (kPA), (d) horizontal wind speed (ms^{-1}), and (e) net radiation (wm^{-2})as measured at KON (gold) and KFB (blue).

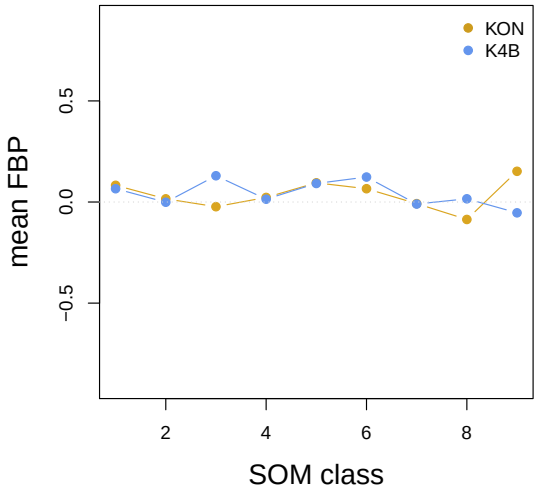

Figure 3.7: Average FBP value of days within each SOM classification. FBP does not differ significantly between sites or between SOM classes.

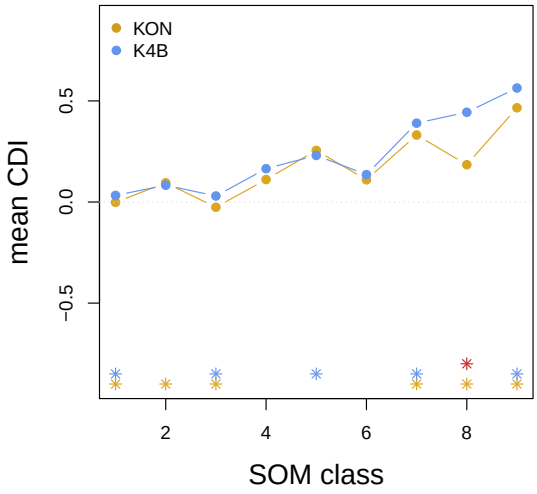

Figure 3.8: Average CDI value of days within each SOM classification. SOM classes in which CDI differs significantly ($p < 0.05$) from the mean CDI at KON/KFB are marked with a gold/blue asterisks and classes in which the distribution of CDI differs significantly between the sites are marked with a red asterisk.

0.56 and 0.47 in class 9 at KON and KFB, respectively. Exceptions to the general trend include a significant drop to 0.18 at KON in class 8 and a decrease at both sites in class 6.

To see how the SOM classes relate to diurnal development and interactions with the PBL, MD of select SOM classes are shown in Figure 3.10. Class 6 is most distinctive for having the highest u (7.9 and 5.8 ms^{-1}) and u_* (0.68 and 0.78 ms^{-1}) at both KON and KFB of any SOM category. The class was not significantly varying between sites in any LA coupling metric, though it did show a drop in CDI at both sites and a significant drop in PTR. MD of this (Figure 3.10a) shows nearly identical average Lq and $C_p\theta$ and development throughout the day. Fluxes are similar between sites for both the surface (β_{sfc} = 0.3 and 0.27 at KON and KFB) and atmospheric (β_{atm} = 1.01 and 0.98 at KON and KFB) components. This may be indicative of strong mixing through the area caused by the strong and turbulent winds. Class 8, which differs between sites for both PTR and CDI, is defined primarily by the opposite conditions: low u (3.3 and 1.8 ms^{-1}) and u_* (0.36 and 0.32 ms^{-1}), but also high T_a (31.4 and 26.7 °C) and net radiation (545 and 536 Wm^{-2}) at KON

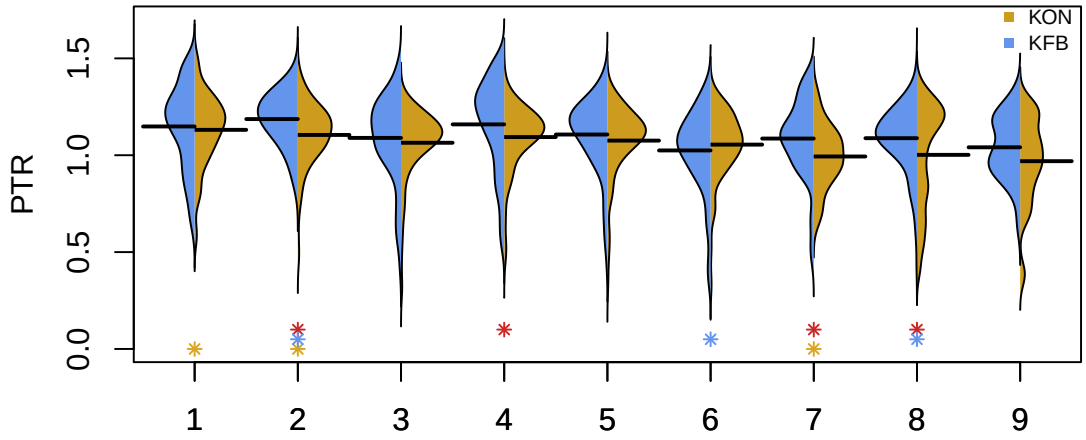

Figure 3.9: Distribution within each SOM classification PTR at KON (gold) and KFB (blue). SOM classes in which PTR differs significantly ($p < 0.05$) from the mean at KON/KFB are marked with a gold/blue asterisks and SOM classes in which the distribution of PTR differs significantly between the sites are marked with a red asterisk.

and KFB. MD show a much greater difference in total energy between sites in these conditions (3.00 and 3.67 kJ/kg difference in mean Lq and $C_p\theta$), though surface flux components do not differ much from class 6 and have no larger a difference between sites (β_{sfc} = 0.29 and 0.26 for KON and KFB). There is, however, a large difference in the atmospheric flux components, with a greater magnitude and a larger proportion of it made up of sensible heating at KFB (β_{atm} = 1.06 at KON and -2.27 at KFB).

Class 7 and 9, both distinct for following long periods without precipitation (8.3 and 14.2 days, respectively), are also plotted (Figure 3.10b). SOM class 9 also has the highest mean temperatures (34.7, 35.4 °C), VPD (3.53, 4.30 kPa) and Rn (569, 578 Wm^{-2}) at KON and KFB, respectively. Class 7 has lower mean T_a (28.0, 23.7 °C), VPD (2.07, 1.25 kPa), and Rn (476, 489 Wm^{-2}). As seen in the MD, the more extreme conditions of class 9 following a longer period without precipitation, result in similar mean daily Lq and $C_p\theta$.Though, β_{sfc} differs from 0.32 at KON and 0.23 at KFB, corresponding to greater surface component of latent heat flux at KFB than KON. β_{sfc} is higher at both KON (0.40) and KFB (0.34) for class 7 than 9. Class 7 has the greatest mean difference in Lq (5.18 kJ/kg) and $C_p\theta$ (3.21 kJ/kg) between sites, with KON having the higher

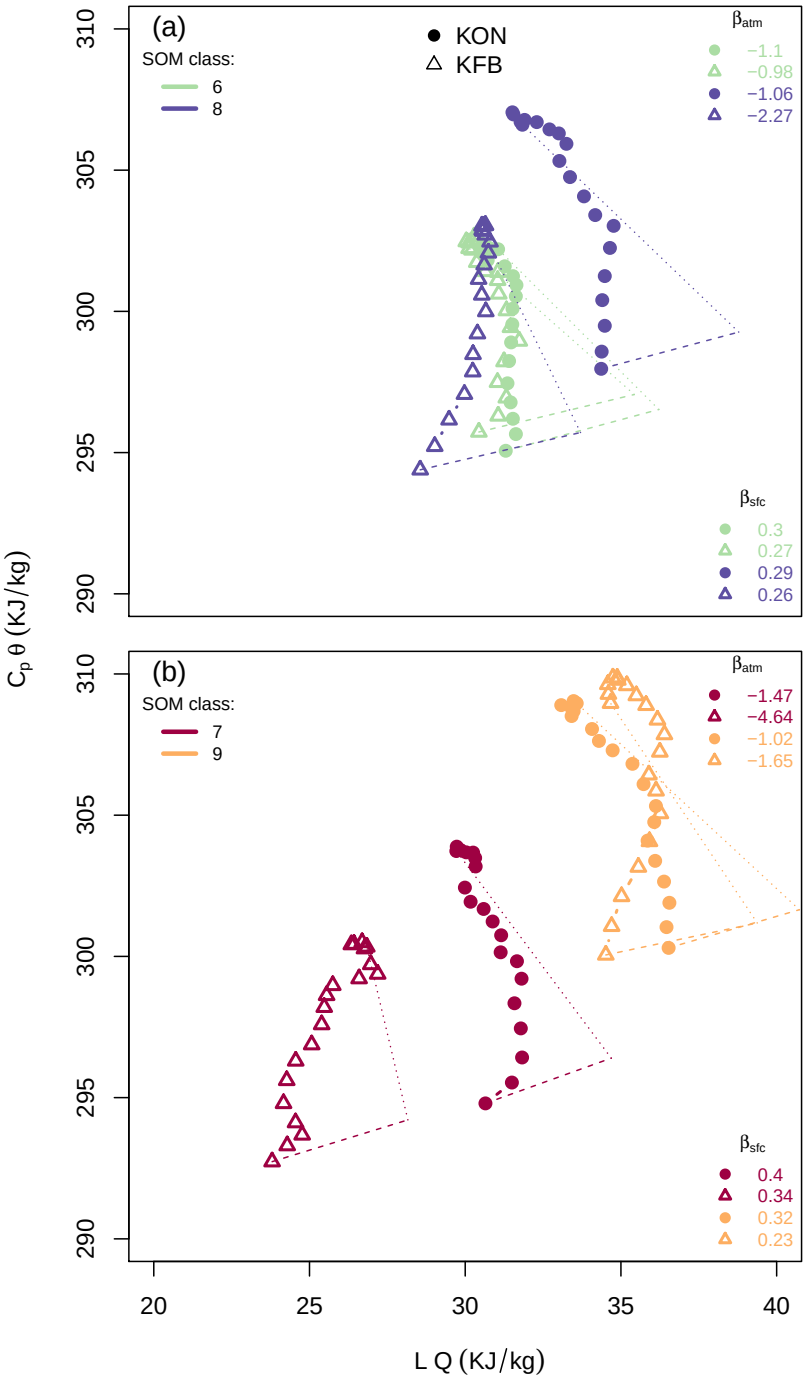

Figure 3.10: Mixing diagrams of mean diurnal development at KON (circles) and KFB (triangles) for select SOM classes: class 6 (teal) and class 8 (purple) in (a); class 7 (dark red) and class 9 (orange) in (b). Total daily flux are decomposed into surface and atmospheric component vectors, shown in dashed and dotted lines, respectively. Also included are the surface (β_{sfc}) and atmospheric (β_{atm}) Bowen ratios for each site and class.

energy. CDI is able to distinguish both class 7 and 9 from their relative means, whereas PTR only picks up a difference in class 7 at KON.

3.4 Discussion

Land surface properties are highly heterogeneous across a range of spatiotemporal scales (e.g. Betts, 2004; Ek & Holtslag, 2004; Brunsell et al., 2011; Reen et al., 2014). Even land covers that would fall within the same category in land surface models, such as the grasslands of this study, can have drastically different responses to the same meteorological forcings based on differences in species' composition, which affects canopy roughness, water-use-efficiency, rooting depth, and other important variables. This study utilizes two closely located EC towers on grassland sites with different burn schedules and consequent plant composition to analyze the impact of this heterogeneity within grasslands on LA interactions and on the utility of a variety of coupling metrics.

To succinctly represent the daytime development of LA interactions, mixing diagrams are used. In MD, the diurnal co-evolution of near-surface specific humidity and potential temperature in energy space are plotted. Plotting MD requires only near-surface temperature and humidity and surface fluxes and then, using PBL height, atmospheric entrainment flux variables that are exceedingly difficult to measure can be estimated (Santanello et al., 2009, 2011; Betts, 1992). Thus, the MD allow for quantification of important components in several steps of a complete LA feedback loop, including those which are not measured directly. The diagrams also include many diagnostics of LA coupling, such as the Bowen ratio of both surface and atmospheric fluxes. MD are plotted for each of the three metrics to determine whether they categorize meaningful differences in surface fluxes and their effects on PBL growth (Figure 3.5b-d).

There are some caveats in the use of MD to infer atmospheric fluxes and estimate entrainment. PBL height, which represents the volume over which the fluxes are scaled, is critical in the calculation of surface flux components and atmospheric response vectors from the residual component (Santanello et al., 2013). Unfortunately, co-located observation of PBL height was not available at the site, so reanalysis product is used, which may introduce some errors in the differentiation

of fluxes into atmospheric and surface components. Even with improved PBL height estimates, another large issue would remain. Presumably, the location of sites less than 1 km apart means they share the same PBL; however, measured fluxes differ between sites, which results in distinctly different estimates of atmospheric response vectors as calculated from residuals in the MD. Large differences between sites in the atmospheric flux component for particular metrics or SOM categories could be largely attributable different days at each site fitting the category, and the differences in the PBL and atmospheric flux on those particular days. However, SOM results indicate that atmospheric flux components are much more similar in conditions that promote strong mixing. Additionally, even when plotted for the same time period, as in Figure 3.5a, the atmospheric flux component varies by a lot, with a difference in β_{atm} of 2.2 between sites. Clearly, there are some issues introduced by using 3 m q and θ measurements as a proxy mixed layer. A large portion of the atmospheric fluxes components, intended to be indicative of entrainment, comes from advection and regional mixing.

Aside from the ability to discern distinct daytime flux developments and atmospheric responses, in order for a metric to be worthwhile it must also contribute some added value beyond what more easily calculated metrics could provide. If, for instance, categorization based solely on soil moisture measurements or meteorological drought can distinguish more substantial differences in LA interactions, it would be pragmatic to stick with the simpler categorization. This study evaluates the relative contribution of metrics in a couple ways. First, metrics of a range of complexity are studied and simple drought/non-drought (Figure 3.5a) and wet/dry soil moisture categorizations are used for comparison. Second, sensitivity of the coupling metrics to meteorological conditions observed at the study sites is tested using SOM. Rather than investigating how the metrics vary with any number of individual meteorological observations, SOM identifies a simplified, comprehensive spectrum of the patterns observed at the sites to be used for analysis.

SOM technique is justified as a useful diagnostic tool as it helps to identify significant structures in the data not just through identifying clusters, but also ensuring identified classes are representative of nearby observations and, when taken together, span the multi-dimensional distribution

function of input data (Hewitson & Crane, 2002; Cavazos, 2000). Another advantage of SOM is that the process is unsupervised, requiring no user assumptions on what the resultant patterns should look like (Kangas & Kohonen, 1996; Kohonen, 1995). The SOM process is used to convert six meteorological variables that are not directly used in any of the coupling metrics into 9 distinct 'classes' which cover the range of conditions seen over the entire period of study. Distribution of input variables within each class is shown in Figure 3.6. Resultant classes can then be used to identify which significant meteorological patterns, if any, the metrics are sensitive to, and which patterns result in different behavior between the sites, thus potentially increasing the impact of heterogeneity on LA coupling feedbacks and the metrics that measure them.

Feedback parameter is the simplest of the three metrics calculated in this study. Based on covariance between soil moisture and precipitation relative to the autocovariance of soil moisture itself, the FBP is meant to cover the entire range of LA coupling. It has been used frequently to approximate land atmosphere coupling strength or quantify the amount of precipitation attributable to soil moisture variability in many regions (e.g. Zeng et al., 2010; Zhang et al., 2008, 2009; Notaro, 2008). Unfortunately, the metric has been shown to potentially inaccurately overestimate the impact of regional soil moisture. A study by Sun & Wang (2012) analyzing the accuracy of FBP looked into the physical mechanisms contributing to precipitation in several regions identified as hotspots of high FBP in global climate models, and concluded that FBP likely usually overestimates the impact of soil moisture on local precipitation. However, the region that includes Konza LTER – the US Great Plains – was identified by Sun & Wang (2012) as the sole hotspot with potentially accurate feedback estimates, because it was the only region of high FBP investigated where ET played a dominant role in precipitation variability and is primarily moisture-limited and where precipitation variability is not dominated by large-scale circulations such as oceanic forcing. Still, their results show that larger-scale circulations can overwhelm the metric and obscure regional feedback between soil moisture and precipitation making FBP inaccurate.

Given that soil moisture and ET can vary significantly between the sites due to differing management practices and resultant vegetation coverage differences, but that precipitation received is

always nearly identical, it is expected that FBP will have significant flaws when calculated at field-scale observations, as done here. Average FBP is somewhat higher at KFB than KON. If the region is expected to have a strong feedback, as many aforementioned studies show, this may simply indicate that KFB is more representative of conditions in the region, where woody encroachment is common (Ratajczak et al., 2012), and that FBP is dominated by these larger-scale, regional feedbacks. This would be expected given the relatively long temporal scale and lag-lead time of covariances used to calculated the FBP. This also implies that heterogeneity in this area may significantly weaken the parameter. Indeed, the most notable feature of the MD of FBP (Figure 3.5c) is that FBP is highest during periods of strong similarity of surface fluxes between sites. When the diverse types of grasslands are behaving similarly in terms of latent and sensible heat fluxes, heterogeneity within the grasslands will not have as much of a dampening factor on any potential feedback. Otherwise, the MD show no meaningful differences in LA interactions captured by the FBP. The FBP also does not show any sensitivity to more complex environmental forcings, with no significant changes across any of the SOM classes or between sites within any class (Figure 3.7).

The second metric evaluated is PTR, a measure of the efficiency of surface evaporation to the PBL. This metric incorporates only one step of the LA interaction chain in detail, rather than attempting to quantify the entire feedback with a single value, but is often used to explore the relationship between many other parameters such as net radiation and soil moisture to surface flux efficiency. PTR is generally interpreted as the ratio between actual evaporation rate and equilibrium evaporation rate (Eichinger et al., 1996). Since entrainment from the top of the PBL will dry the mixed layer and allow for more evaporation, PTR is actually expected to be above 1 in non-water-stressed conditions. Values are shown to range between 1.2 and 1.3 over vegetation in the absence of water stress (Priestley & Taylor, 1972; Raupach, 2001; Betts, 2004; van Heerwaarden et al., 2009). Lower values of PTR are caused by water-limited conditions and higher values are caused by stronger entrainment, reduced aerodynamic resistance, and/or increased canopy resistance. Results show PTR is very similar at KON and KFB for the first three years of the study (2008 - 2010), reaching expected peak efficiencies of between 1.2 and 1.3 each growing season

(Figure 3.2). For the next two years, strong droughts occur (beginning in June 2011 and May 2012). At this point PTR rapidly decreased to well below 1 at both sites. However, the decrease is less steep for KFB and the site recovers to near-peak values in late summer. Afterwards, PTR values tend to be higher at KFB (averaging 0.2 higher than at KON), and the site continues to show a dampened response to, and faster recovery from drought conditions.

These temporal patterns observed in PTR correspond to changes in vegetation composition that occurred at KFB over the period of observation. Konza LTER site has historically been devoid of woody vegetation outside riparian areas, but woody encroachment has been occurring in sites with a managed burn frequency of 3 years or more (Ratajczak et al., 2011). KFB, burned every 4 years, has experienced large expansion in shrub coverage, to over 50%. KON, burned annually, has experienced no similar changes in vegetation. The dogwood shrubs that make up the majority of woody encroachment in the area, have been shown to access deeper sources of soil moisture. While the dominant grasses at Konza LTER draw water almost exclusively from the first 25 cm of soil, dogwood draws primarily from depths greater than 30 cm (Ratajczak et al., 2011; Nippert & Knapp, 2007b). A previous study finds that these changes in root access to moisture greatly alter ET response to soil moisture conditions and drought (Logan & Brunsell, 2015). The changes in PTR between sites with drought mirrors these earlier results. The subsequent shift of PTR to higher values at KFB even after drought conditions have receded may be indicative of changes in canopy resistance with changing species composition and increased heterogeneity. Woody encroachment increases spatial variance and roughness as patches of fire-resistant shrubs grow (Ratajczak et al., 2016). The differences in mean PTR between sites peaks in 2013, when both sites underwent managed burns but KFB was largely covered in patches of fire-resistant dogwood.Although PTR demonstrates great sensitivity to changes in plant composition, it does not significantly vary with sites between many of the range of environmental conditions identified with SOM. Between sites, however, PTR differs significantly for classes that highlight the heterogeneity between sites and produce distinctly difference surface flux conditions.

MD show that PTR is able to isolate the largest differences in surface fluxes of any of the

metrics (Figure 3.5b). High PTR values have a much larger magnitude of moisture flux into the atmosphere, corresponding to a very low β_{sfc} and low PTR have the opposite, with large sensible heating and very little latent heat flux. This differentiation is to be expected, because PTR incorporates the evaporative fraction (EF), which is directly related to β (EF = $\frac{1}{1+\beta}$). At KON, simple categorization by drought/non-drought summers is able to produce similar results (Figure 3.5a) with similar diurnal co-evolution of q and θ as low/high PTR. PTR, however, is able to identify similarly distinct daytime flux patterns at KFB, while drought categorization is not. During summers in which drought occurred, daytime fluxes at KFB are very similar to normal conditions due to the changes in plant cover and resultant dampened response to drought mentioned above. This is displayed clearly in the MD, with nearly identical q and θ conditions for much of the day, only differing by greater overall increase in energy during drought coming from increased sensible heating in both the surface and atmospheric components. MD of classification by highest/lowest 10^{th} percentile of soil moisture as measured at the EC tower sites have the same lack of differentiation in dry conditions at the grassland experiencing woody encroachment. Since the encroaching shrubs have access to soil moisture at depths greater than 30cm, the simple classifications would likely remain bad at characterizing differences in LA interactions unless measured to greater depths. PTR is ideally suited to EC towers and, where flux measurements are available, has added value in differentiation of LA interactions.

The third LA coupling metric assessed is CDI. Rather than high/low feedback strength, CDI is divided into coupling regimes based on local soil moisture statistics in the CTP-HI space, and the potential for evaporation and for moisture to drive precipitation. Since it is calculated as daily values based on historical soil moisture statistics, CDI allows for temporal and real-time assessment of the sensitivity of convection to local land-surface conditions (Santanello et al., 2017). Roundy et al. (2013) found that wet and dry coupling states correspond to distinct equilibria of soil moisture and show strong persistence, connected to changes in both the frequency and depth of precipitation. A CDI dataset developed using AIRS sounding data is used in this study (Roundy & Santanello, 2017). Differences in spatial and temporal scale must be kept in mind when com-

paring CDI to the metrics calculated with EC tower data. The proximity of the study sites and 1° resolution of AIRS data mean that KON and KFB always having the same coupling classification, and thus identical CDI values, though flux measurements will vary between sites within the same classification. MD of CDI can thus be used to view how LA interactions differ in grasslands with woody encroachment within the same coupling regime.

Climatological CDI in the area has a strong seasonal pattern, with wet coupling conditions dominating in winter and early spring and dry coupling in the summer and early fall (Figure 3.4). MD classifications are calculated using deviations of 7-day CDI from the 30-year mean to compare unusually persistent wet and dry conditions rather than seasonal variations. CDI does distinguish distinct patterns of daytime evolutions of energy at both study sites, with consistent increases in θ and q during wet coupling and similar increases θ but strong afternoon drying during dry coupling (Figure 3.5d). This pattern is largely due to the atmospheric response component. Although dry coupling has larger surface latent heat fluxes than wet, the atmospheric contribution is even stronger drying and warming, consistent with deep PBL growth and entrainment of warm, dry air at the top of the PBL. This influx of warm, dry air raises atmospheric demand, increasing surface evapotranspiration which could deplete soil moisture and, assuming atmospheric demand is too high to trigger convective precipitation, support further drying. This overall pattern is similar to modeled results for dry soils and dry regimes (Santanello et al., 2011, 2013).

In the aforementioned studies, 'wet regime' correspond to higher starting $Cp\theta$ and Lq, a daytime pattern of moistening with very little warming, and very low surface β_{sfc}, resulting in limited PBL growth and entrainment. Wet coupling conditions, as defined by CDI deviations and measured at the EC towers, differ more significantly from these modeling studies. β_{sfc} is higher for low (wet) CDI than high, overall energy is lower, including much lower Lq, and the magnitude of daytime heating is similar. The disparity in total energy may be simply due to the seasonality of wet and dry deviations in CDI over the study period. Deviations of high CDI occur most frequently in late-summer when total energy will be higher. One similarity to what is modeled over wet soils is the strong surface latent heat flux resulting in overall daytime increases in Lq. During wet coupling,

there is more latent heat flux from the surface than from the atmosphere at both KON and KFB. The higher sensible heat flux, nearly equivalent to that seen during dry coupling, may be caused by differences in the definition of wet coupling regime in CDI corresponding to not just high soil moisture, but also convective potential of the atmospheric profile, favoring conditions that create growth in the PBL while still able to meet the moisture demands of the atmosphere.

CDI does appear to be sensitive to a variety of environmental conditions, varying significantly with the majority of SOM classes at both sites (Figure 3.8). It also significantly varies between more classes than soil moisture alone, indicating that the variation with class cannot be solely attributed to the dependence of CDI classification on local soil moisture. CDI generally increases with increasing SOM class, which are ordered by increasing VPD at KON and correlate with increasing T_a and Rn. These conditions match with increased incidence of dry coupling. One exception is class 6, defined by the highest u and u_*, having a drop in CDI, which could correspond to more wet coupling associated with the presumably strong regional mixing, or more transitional or atmospherically controlled coupling, as all other types of classification or missing values cause a CDI to move closer to zero. Coupling regime only significantly differs between the annually burned grassland and one experiencing woody encroachment in SOM class 8, where net radiation and air temperature are relatively high, wind conditions are calm, and it has not been long since precipitation last occurred. These conditions would emphasize differences in surface energy balance based on land cover heterogeneity, because high net radiation highlights contrasts in albedo and plant activity and calm winds result in a lack of mixing across the area. Since this field-scale heterogeneity cannot be directly captured by CDI, which, due to its resolution, is always the same at both sites, the deviation must be caused by a significant mismatch between sites in days which classify as this meteorological pattern. CDI at KON is 0.29 lower (more wet coupling), but given the overall trend in CDI with SOM class and the specific conditions of the class, a higher CDI would be expected. This deviation could be caused by KON more frequently reaching the higher temperatures and VPDs characteristic of the class while the larger, surrounding region is under conditions that coincide with the wet coupling regime, causing a misidentification of CDI at KON.

This would also indicate that the site experiencing woody encroachment is more representative of regional LA coupling.

3.5 Summary and Conclusions

In this study, three LA coupling metrics spanning a range of complexity have been applied to long-term EC tower observations at two proximate grassland sites with different management strategies and consequent divergent ecosystem development. Most LA coupling metrics integrate several parts of the LA coupling chain by necessity. However, this may mask flaws in the metric through confounding errors offsetting each other. Accuracy and utility of the metrics is analyzed using methods that focus on covering the complexity of LA interactions and ensuring process-level understanding.

To analyze the entire daytime development of LA interactions and quantify several aspects of the LA feedback chain, mixing diagrams are used. Despite some caveats in the quantification of atmospheric fluxes from EC tower data, MD prove to be a useful tool for succinctly visualizing daytime changes in near-surface conditions and estimating their impact on the PBL. MD are plotted for the highest and lowest 10^{th} percentile of each of the three metrics at both sites to determine whether they are able to categorize distinct, meaningful differences in surface fluxes and their effects on PBL growth, and to investigate whether heterogeneity between the grassland sites alters these LA interactions or the capability of the metrics.

To ascertain their added value beyond simple soil moisture measurements or drought classification, the range of metrics are compared to those simple categorizations. Additionally, sensitivity of the coupling metrics to more complex meteorological conditions is tested using SOM. The SOM technique is justified as a useful diagnostic tool as it is unsupervised, requiring very few assumptions from the user, and identifies significant patterns that span the distribution of the input data.

Of the three metrics, the feedback parameter is the simplest and found to be least useful. FBP is based on covariances between soil moisture and precipitation. One of these variables (soil moisture) is quite variable between sites due to soil heterogeneity and differing plant composition be-

tween sites, while the other (precipitation) is nearly identical due to their proximity. The result is that FBP calculated based on observational point-data has a very large variance with site selection shows no significant differences with any of the meteorological conditions identified by SOM. MD did not reveal any meaningful differences in LA interactions, aside from perhaps high FBP being associated with stronger similarity in surface conditions and fluxes. Other studies have shown that larger-scale circulations can overwhelm the metric and obscure regional feedback between soil moisture and precipitation making FBP inaccurate. This suggests that FBP might be higher when the diverse types of grasslands are behaving similarly in terms of surface fluxes. However, this distinction in the MD is too small to assume any significance in this result.

The second metric evaluated, PTR, incorporates only one step of the LA interaction chain in detail, rather than attempting to quantify the entire feedback with a single value. PTR is generally interpreted as the ratio between actual evaporation rate and equilibrium evaporation. PTR is very similar at the sites for the first three years of the study, reaching similar and expected peak efficiencies during the growing seasons. During drought, however, the sites diverge and PTR at the site experiencing woody encroachment is able to remain higher and recover faster than the annually burned grassland, which has a precipitous decline. This matches previous study results that show a dampened response to drought with woody encroachment in the region, due to root access to deeper sources of soil moisture from the predominant encroaching shrub. After these droughts, and intensive woody encroachment, PTR values tend to remain higher at KFB than KON and the site continues to show a dampened response to drought conditions.

The dampened response to drought also shows up in MD. Surface conditions and fluxes are nearly identical for high/low soil moisture and drought/non-drought summers at KFB. PTR, however, is able to distinguish much more distinct daytime evolutions than the simpler classifications. In fact, PTR is able to isolate the largest differences in surface fluxes. This differentiation is expected, because PTR directly includes surface bowen ratio in the calculation. PTR also differs significantly between SOM classes that are not conducive to mixing and produce distinctly difference surface fluxes. However, differences within each site across the spectrum of environmental

conditions are less distinct, with PTR seeming to peak after a relatively low threshold of conditions conducive to plant activity is reached, and varying little above that. Overall, PTR has significant differences between sites in more SOM states, but less differences between states. This may indicate that the metric is more sensitive to the differences between plant composition, but less able to discriminate between important meteorological patterns and their impact on boundary layer growth and potential precipitation conditions.

The final and most complex LA coupling metric assessed is CDI. CDI is divided into coupling regimes based on local soil moisture statistics in the CTP-HI space. Wet and dry coupling states correspond to distinct equilibria of soil moisture and show strong persistence, connected to changes in both the frequency and depth of precipitation. CDI in the area has a strong seasonal pattern, with wet coupling conditions dominating in winter and early spring and dry coupling in the summer and early fall. Although not as distinctly as PTR, MD show CDI does distinguish differing patterns of daytime evolutions of energy at both study sites. During dry coupling, both sites show large amounts of sensible heating and strong afternoon drying, largely from the atmospheric contribution. This pattern is consistent consistent with deep PBL growth and entrainment of warm, dry air at the top of the PBL and is similar to the overall pattern found in modeled results over dry soils and dry regimes (e.g. Santanello et al. 2011, 2013). During wet coupling conditions, results differ more substantially from these modeling studies. Overall energy is lower, likely due to the seasonal timing of strong deviations of wet and dry coupling. Sensible heat flux is also much higher, nearly equivalent to that seen during dry coupling. This pattern may be caused by differences in the definition of 'wet coupling' in CDI. CDI is based not just on high soil moisture, but also on convective potential of the atmospheric profile over wet soils, and seems to include conditions that create more growth in the PBL, while keeping latent energy high as well.

CDI is also sensitive to a variety of environmental conditions, varying significantly with the majority of SOM classes at both sites. However, it does not distinguish many differences between sites due to the scale of the metric. CDI is always the same at both sites, so any significant deviations between sites have to be caused by a significant mismatch in days which fall into that

meteorological pattern. Coupling regime only significantly differs between the annually burned grassland and one experiencing woody encroachment in one SOM class that has conditions which emphasize differences in surface energy balance based on land cover heterogeneity. The deviation between sites is thought to be caused by KON more frequently reaching the higher temperatures and VPDs characteristic of the SOM class while the larger, surrounding region is under conditions that coincide with the wet coupling regime, causing a misidentification of CDI at KON. This result suggests that the site experiencing woody encroachment is more representative of larger, regional conditions and coupling regime.

Chapter 4

Conclusions

4.1 Summary of Findings

Interactions between the land surface and atmosphere are a large part of the water and energy budgets at the surface. They modulate near-surface climate, including precipitation, and feedbacks between them can influence the persistence of extreme events like drought. Yet these interactions remain a weak point in our understanding of the Earth's climate system and contribute to uncertainty in projections of future climate. This is due in large part to the high spatiotemporal variability of land cover, the complexity of LA interactions, and the difficulty of gathering a complete set of observations at the needed temporal and spatial. The research included in this dissertation attempts to address the first two issues over a central US grassland. The influence of spatiotemporal variability is investigated through comparison between two proximate grassland sites with differing land cover across a range of time scales and over a lengthy time series of observations that cover a range of environmental forcings. The complexity of interactions is covered by utilizing a wide variety of LA feedback metrics and analysis tools that allow for investigation of several steps and causal linkages in the LA feedback chain.

Chatper 2 examines daytime turbulent fluxes throughout the growing season during two wet years and one drought year. Results show that the site experiencing more woody encroachment was a much greater carbon sink every year, with CO_2 flux into the ecosystem nearly doubling and tripling that of the annually burned grassland in the study years with high precipitation. During drought, this difference is exacerbated, with the annually burned grassland becoming a likely source of carbon. Woody encroachment also yielded greater seasonal water-use efficiency (WUE)

during normal or high precipitation conditions, except over the period of spring burning. During drought, however, there was evidence of depletion of deeper, stored water resources with woody encroachment as cumulative evaporative loss surpassed cumulative annual precipitation at KFB. Root access of the encroaching shrub species to deeper soil moisture results in greater photosynthesis occurring during otherwise drier conditions, which results in increased productivity and decreased WUE.

Changes in the nature of the turbulent fluxes were also investigated through deviations from similarity theory, quadrant analysis, and wavelet decomposition. Wavelet analysis determined the size of eddies primarily involved in net exchange, showing differences between sites across small to medium scales. Eddy size decrease over the course of the growing season occurs in a strikingly inverse relation to grass leaf area index, likely corresponds to greater canopy height and roughness. Between sites, smaller eddy size of maximum transport and slightly weakened applicability of similarity theory at KFB likely corresponds to increased surface heterogeneity and roughness with woody encroachment. Variance of the correlation of carbon and water fluxes, indicative of more variable plant productivity, is much greater across all scales of motion during drought at KON only.

Overall, results of Chapter 2 indicate that woody encroachment increases resilience to drought due to changes in root access to soil moisture and alterations in the canopy structure. These results suggest that on a regional scale, increases in woody encroachment with human-driven land cover changes have caused increased carbon sequestration and ecosystem WUE during non-drought conditions. Given the projected increases in aridity with climate change, this would be a welcome shift. However, this study also indicates that in times of water stress, the benefit of woody encroachment-induced increases in WUE disappear and greater depletion of stored groundwater may occur, which could prove detrimental in combination with predicted increases in aridity.

In Chapter 3, three LA coupling metrics spanning a range of complexity and looking at different segments of the LA coupling chain were applied to observations at the grassland sites. Additionally, accuracy and utility of the metrics were analyzed using two methods that focus on covering the complexity of LA interactions and ensuring process-level understanding. First, a comprehensive

range of significant meteorological patterns that occur at the site are identified using self-organizing maps. The sensitivity of coupling metrics to SOM classes is used to diagnose their ability to detect differences in LA interactions inherent in these distinct patterns. Second, mixing diagrams are used to succinctly visualize the entire daytime evolution of near-surface energy and to quantify several important properties of the surface and atmospheric flux components. MD of average diurnal evolution by metric categorization provide information on whether the metrics are separating distinct surface conditions with meaningful differences in PBL response.

The three metrics considered are: the feedback parameter, Priestley-Taylor Ratio, and Coupling Drought Index. FBP is the simplest metric, based on statistical relationships between soil moisture and precipitation, and is found to be the least effective. FBP calculated based on small-scale is very dependent on site selection and shows no significant differences with any of the meteorological conditions identified by SOM or identification of distinct LA interactions in MD for high or low feedback. FBP may be higher when surface conditions are more similar between the sites, indicating this metric is dominated by larger-scale

PTR investigates only one step of the LA interaction chain in detail, rather than attempting to quantify the entire feedback with a single value. PTR is able to isolate the largest differences in surface energy partitioning by definition, and this distinction shows up clearly in the MD. However, the metric is not very useful for detecting differences across the spectrum of environmental conditions, seeming to peak after a relatively low threshold of conditions conducive to plant activity and vary little above that. PTR does vary with changing species' composition between sites, though, starting out similar but behaving much differently during drought, reflective of the dampened response to drought seen at KFB in Chapter 2. After drought conditions end, there remains a significant difference between sites indicative of the changes to canopy structure due to increased woody encroachment at KFB. Overall, the metric is more sensitive to the differences between plant composition, but less able to discriminate between important meteorological patterns and their impact on boundary layer growth and potential precipitation conditions.

The final and most complex LA coupling metric assessed is CDI. It divides conditions into

coupling regime based on local soil moisture statistics in the CTP-HI space that are associated with continued or intensified deviations in kind in soil moisture. CDI has a strong seasonal pattern and is also sensitive to a wide variety of meteorological patterns at both sites. MD show CDI does distinguish differing, meaningful patterns of daytime evolutions of energy at both study sites. During dry coupling, both sites show large amounts of sensible heating and strong afternoon drying, largely from the atmospheric contribution, consistent with deep PBL growth and entrainment of warm, dry air at the top of the PBL. The wet coupling classification seems to favor conditions conducive to some growth of the PBL while keeping humidity relatively high.

However, CDI does not distinguish many differences between sites. Due to the scale of the metric, any significant deviations between sites must be caused by a significant mismatch in days which fall into that meteorological pattern. Results indicate that this occurs under conditions which emphasize differences in surface energy balance based on land cover heterogeneity. In these cases, designated coupling regime corresponds to conditions seen at the site experiencing woody encroachment, suggesting that surface fluxes there are more representative of larger, regional conditions. Overall, results in chapter 3 highlights the need to carefully consider scale and objective when selecting a metric of LA coupling strength.

4.2 Summary of Contributions

The dissertation builds on a large body of research in how changes in grassland composition and encroaching herbaceous and woody plant species can alter regional carbon and water budgets through alterations of productivity, WUE, source water depth, and turbulent flux dynamics. Results fall in line the findings of many other studies of carbon source/sink status of grasslands (e.g. Schwalm et al. 2010; Aires et al. 2008; Meyers 2001). In terms of the hydrological cycle, this research supports findings by Brunsell et al. (2014) of greater WUE with woody encroachment, despite the generally higher leaf-level WUE of C_4 grasses (Ehleringer & Monson, 1993). Previous research has shown that woody encroachment can result in increased groundwater usage (Scott et al., 2006), and stable isotope analysis has indicated that dogwood patches pull from deeper sources of soil

moisture (Nippert & Knapp, 2007a). Results presented in this dissertation support these findings and help quantify their impact on the hydrological cycle through surface fluxes measurements. This dissertation also expands on the well-researched changes in the carbon, water, and energy cycles with changing grasslands, by investigating how these overall changes are manifested in the surface turbulence.

The International Global Energy and Water Exchanges project (GEWEX) Global Land- Atmosphere System Study (GLASS) formed a Local LA Coupling project to examine LA interactions at the local process level. Santanello et al. (2017) asserts that the most prominent contribution of the project has been development and promotion of LA coupling metrics to diagnose coupling between the local land surface, PBL, and precipitation coupling. This dissertation research attempts to build on that work by assessing the accuracy and utility of many of these metrics under a variety of conditions. Mixing Diagrams are, for the first time, utilized in comparison between observational data and to diagnose the effectiveness of other metrics of LA interactions and feedbacks. MD are shown to be a useful tool for investigating the totality of LA interactions, even for observational data that is naturally less spatially and temporally complete than model output. This research also includes the first time self-organizing maps are used in the investigation of the sensitivity of LA feedback metrics.

4.3 Recommendations for Future Work

The research presented in this dissertation highlights the need to include land cover heterogeneity and changes in species composition in forecasts of the impacts of climate change on carbon sequestration, the local water budget, and energy partitioning. Changes in climate forcings that push a region past an ecosystem tipping point of could drastically alter local LA interactions and result in changing feedbacks that could, in turn, alter the initial climate predictions. Ideally, some consideration of heterogeneity would be included in LSM to account for the variability in LA interactions found within the individual categories of land cover.

Given the usefulness of mixing diagrams in evaluating the complete LA feedback. Expansion

of observational platforms to include measurements of planetary boundary-layer height co-located with EC towers at more locations is recommended. These observations would also help fill in the gaps of observational data, with observations spanning from the land surface to top of PBL across a wider variety of land covers. The need for this is clear, as over-reliance on observational data from a few select study sites (such as SGP) and model inter-comparison has been identified as a potential cause of the relatively poor performance of land surface models, and our results highlight the large influence small changes in land cover can have.

References

Abramowitz, G. (2012). Towards a public, standardized, diagnostic benchmarking system for land surface models. *Geosci. Model Dev.*, 5(3), 819–827.

Aires, L., Pio, C., & Pereira, J. S. (2008). Carbon dioxide exchange above a Mediterranean C3/C4 grassland during two climatologically contrasting years. *Global Change Biol*, 14(3), 539–555.

Antonia, R. A. (1981). Conditional sampling in turbulence measurement. *Annual Review of Fluid Mechanics*, 13(1), 131–156.

Baldocchi, D., Falge, E., Gu, L., Olson, R., Hollinger, D., Running, S., Anthoni, P., Bernhofer, C., Davis, K., & Evans, R. (2001). FLUXNET: A new tool to study the temporal and spatial variability of ecosystem-scale carbon dioxide, water vapor, and energy flux densities. *Bull. Amer. Meteor. Soc.*, 82(11), 2415–2434.

Barger, N. N., Archer, S. R., Campbell, J. L., Huang, C.-y., Morton, J. A., & Knapp, A. K. (2011). Woody plant proliferation in North American drylands: A synthesis of impacts on ecosystem carbon balance. *J. Geophys. Res.*, 116, G00K07.

Best, M. J., Abramowitz, G., Johnson, H. R., Pitman, A. J., Balsamo, G., Boone, A., Cuntz, M., Decharme, B., Dirmeyer, P. A., Dong, J., Ek, M., Guo, Z., Haverd, V., van den Hurk, B. J. J., Nearing, G. S., Pak, B., Peters-Lidard, C., Santanello Jr, J. A., Stevens, L., & Vuichard, N. (2015). The Plumbing of Land Surface Models: Benchmarking Model Performance. *J. Hydrometeor*, 16(3), 1425–1442.

Betts, A. K. (1992). FIFE atmospheric boundary layer budget methods. *J. Geophys. Res. Atmos.*, 97(D), 18,523–18,531.

Betts, A. K. (1994). Relation between equilbrium evaporation and the saturation pressure budget. *Boundary-Layer Meteorol*, 71(3), 235–245.

Betts, A. K. (2004). Understanding Hydrometeorology Using Global Models. *Bull. Amer. Meteor. Soc.*, 85(11), 1673–1688.

Blair, J. M., Nippert, J. B., & Briggs, J. M. (2013). Grassland Ecology. In R. Monson (Ed.), *In The Plant Sciences - Ecology and the Environment* (pp. 1–28). Verlag Berlin Heidelberg: Springer.

Bou-Zeid, E., Meneveau, C., & Parlange, M. B. (2004). Large-eddy simulation of neutral atmospheric boundary layer flow over heterogeneous surfaces: Blending height and effective surface roughness. *Water Resour. Res.*, 40(2), W02505.

Bowling, D. R., Bethers-Marchetti, S., Lunch, C. K., Grote, E. E., & Belnap, J. (2010). Carbon, water, and energy fluxes in a semiarid cold desert grassland during and following multiyear drought. *J. Geophys. Res.*, 115(G4), G04026.

Bremer, D. J. & Ham, J. M. (2010). Net carbon fluxes over burned and unburned native tallgrass prairie. *Rangeland Ecology & Management*, 63(1), 72–81.

Brunsell, N. A. (2006). Characterization of land-surface precipitation feedback regimes with remote sensing. *Remote Sensing of Environment*, 100(2), 200–211.

Brunsell, N. A., Mechem, D. B., & Anderson, M. C. (2011). Surface heterogeneity impacts on boundary layer dynamics via energy balance partitioning. *Atmos. Chem. Phys.*, 11(7), 3403–3416.

Brunsell, N. A., Nippert, J. B., & Buck, T. L. (2014). Impacts of seasonality and surface heterogeneity on water-use efficiency in mesic grasslands. *Ecohydrology*, 7(4), 1223–1233.

Cava, D., Katul, G. G., Sempreviva, A. M., Giostra, U., & Scrimieri, A. (2008). On the Anomalous Behaviour of Scalar Flux–Variance Similarity Functions Within the Canopy Sub-layer of a Dense Alpine Forest. *Boundary-Layer Meteorol*, 128(1), 33–57.

Cavazos, T. (2000). Using Self-Organizing Maps to Investigate Extreme Climate Events: An Application to Wintertime Precipitation in the Balkans. *J. Climate*, 13(10), 1718–1732.

Christensen, J. H., Hewitson, B., Busuioc, A., Chen, A., Gao, X., Held, R., Jones, R., Kolli, R. K., Kwon, W. K., Laprise, R., V., M. R., Mearns, L., Menendez, C., Raisanen, J., Rinke, A., Sarr, A., & Whetton, P. (2007). Regional climate projections. *Climate Change, 2007: The Physical Science Basis. Contribution of Working group I to the Fourth Assessment Report of the Intergovernmental Panel on Climate Change, University Press, Cambridge, Chapter 11*, (pp. 847–940).

Dai, A. (2012). Increasing drought under global warming in observations and models. *Nature Climate Change*, 3(1), 52–58.

Davin, E. L., Maisonnave, E., & Seneviratne, S. I. (2016). Is land surface processes representation a possible weak link in current Regional Climate Models? *Environ. Res. Lett.*, 11(7), 074027.

Dee, D. P., Uppala, S. M., Simmons, A. J., Berrisford, P., Poli, P., Kobayashi, S., Andrae, U., Balmaseda, M. A., Balsamo, G., Bauer, P., Bechtold, P., Beljaars, A. C. M., van de Berg, L., Bidlot, J., Bormann, N., Delsol, C., Dragani, R., Fuentes, M., Geer, A. J., Haimberger, L., Healy, S. B., Hersbach, H., Hólm, E. V., Isaksen, L., Kållberg, P., Köhler, M., Matricardi, M., McNally, A. P., Monge-Sanz, B. M., Morcrette, J. J., Park, B. K., Peubey, C., de Rosnay, P., Tavolato, C., Thépaut, J. N., & Vitart, F. (2011). The ERA-Interim reanalysis: configuration and performance of the data assimilation system. *Q.J.R. Meteorol. Soc.*, 137, 553–597.

Detto, M., Katul, G., Mancini, M., Montaldo, N., & Albertson, J. D. (2008). Surface heterogeneity and its signature in higher-order scalar similarity relationships. *Agricultural and Forest Meteorology*, 148(6-7), 902–916.

Dirmeyer, P. A., Gao, X., Zhao, M., Guo, Z., Oki, T., & Hanasaki, N. (2006). GSWP-2: Multimodel Analysis and Implications for Our Perception of the Land Surface. *Bull. Amer. Meteor. Soc.*, 87(10), 1381–1397.

Dirmeyer, P. A., Jin, Y., Singh, B., & Yan, X. (2013). Evolving Land–Atmosphere Interactions over North America from CMIP5 Simulations. *J. Climate*, 26(19), 7313–7327.

Ehleringer, J. R. & Monson, R. K. (1993). Evolutionary and ecological aspects of photosynthetic pathway variation. *Annual Review of Ecology and Systematics*, (pp. 411–439).

Eichinger, W. E., Parlange, M. B., & Stricker, H. (1996). On the Concept of Equilibrium Evaporation and the Value of the Priestley-Taylor Coefficient. *Water Resour. Res.*, 32(1), 161–164.

Ek, M. B. & Holtslag, A. (2004). Influence of soil moisture on boundary layer cloud development. *J. Hydrometeor*, 5(1), 86–99.

Falge, E., Baldocchi, D., Olson, R., Anthoni, P., Aubinet, M., Bernhofer, C., Burba, G., Ceulemans, R., Clement, R., & Dolman, H. (2001). Gap filling strategies for defensible annual sums of net ecosystem exchange. *Agricultural and Forest Meteorology*, 107(1), 43–69.

Farge, M. (1992). Wavelet transforms and their applications to turbulence. *Annual Review of Fluid Mechanics*, 24(1), 395–458.

Ferguson, C. R. & Wood, E. F. (2011). Observed Land-Atmosphere Coupling from Satellite Remote Sensing and Reanalysis. *J. Hydrometeor*, 12, 1221–1254.

Findell, K. L. (2003). Atmospheric controls on soil moisture-boundary layer interactions: Three-dimensional wind effects. *J. Geophys. Res.*, 108(D8), 8385.

Findell, K. L. & Eltahir, E. A. (2003a). Atmospheric controls on soil moisture-boundary layer interactions. Part I: Framework development. *J. Hydrometeor*, 4(3), 552–569.

Findell, K. L. & Eltahir, E. A. (2003b). Atmospheric controls on soil moisture-boundary layer interactions. Part II: Feedbacks within the continental United States. *J. Hydrometeor*, 4(3), 570–583.

Findell, K. L., Gentine, P., Lintner, B. R., & Kerr, C. (2011). Gentine, 2011 Probability of afternoon. *Nature Geoscience*, 4(6), 1–6.

Finnigan, J. (2000). Turbulence in plant canopies. *Annual Review of Fluid Mechanics*, 32(1), 519–571.

Flato, G., Marotzke, J., Abiodun, B., Braconnot, P., Chou, S. C., Collins, W. J., Cox, P., Driouech, F., Emori, S., Eyring, V., et al. (2013). Evaluation of climate models. in: climate change 2013: the physical science basis. contribution of working group i to the fifth assessment report of the intergovernmental panel on climate change. *Climate Change 2013*, 5, 741–866.

Foken, T. (2006). 50 Years of the Monin–Obukhov Similarity Theory. *Boundary-Layer Meteorol*, 119(3), 431–447.

Francone, C., Katul, G. G., Cassardo, C., & Richiardone, R. (2012). Turbulent transport efficiency and the ejection-sweep motion for momentum and heat on sloping terrain covered with vineyards. *Agricultural and Forest Meteorology*, 162-163, 98–107.

Frankignoul, C. & Hasselmann, K. (1977). Stochastic climate models, part ii application to sea-surface temperature anomalies and thermocline variability. *Tellus*, 29(4), 289–305.

Harding, K. J. & Snyder, P. K. (2012a). Modeling the Atmospheric Response to Irrigation in the Great Plains. Part I: General Impacts on Precipitation and the Energy Budget. *J. Hydrometeor*, 13(6), 1667–1686.

Harding, K. J. & Snyder, P. K. (2012b). Modeling the Atmospheric Response to Irrigation in the Great Plains. Part II: The Precipitation of Irrigated Water and Changes in Precipitation Recycling. *J. Hydrometeor*, 13(6), 1687–1703.

Haughton, N., Abramowitz, G., Pitman, A. J., Or, D., Best, M. J., Johnson, H. R., Balsamo, G., Boone, A., Cuntz, M., Decharme, B., Dirmeyer, P. A., Dong, J., Ek, M., Guo, Z., Haverd, V., van den Hurk, B. J. J., Nearing, G. S., Pak, B., Santanello Jr., J. A., Stevens, L. E., & Vuichard, N. (2016). The Plumbing of Land Surface Models: Is Poor Performance a Result of Methodology or Data Quality? *J. Hydrometeor*, 17(6), 1705–1723.

Hewitson, B. C. & Crane, R. G. (2002). Self-organizing maps: applications to synoptic climatology. *Climate Research*, 22(1), 13–26.

Hillel, D. (1998). *Environmental soil physics: fundamentals, applications, and environmental considerations*. Academic press.

Huber, D., Mechem, D., & Brunsell, N. (2014). The Effects of Great Plains Irrigation on the Surface Energy Balance, Regional Circulation, and Precipitation. *Climate*, 2(2), 103–128.

Hufkens, K., Keenan, T. F., FLANAGAN, L. B., Scott, R. L., Bernacchi, C. J., Joo, E., Brunsell, N. A., Verfaillie, J., & RICHARDSON, A. D. (2016). Productivity of North American grasslands is increased under future climate scenarios despite rising aridity. *Nature Climate Change*.

Huxman, T. E., Wilcox, B. P., Breshears, D. D., Scott, R. L., Snyder, K. A., Small, E. E., Hultine, K., Pockman, W. T., & Jackson, R. B. (2005). Ecohydrological implications of woody plant encroachment. *Ecology*, 86(2), 308–319.

Jackson, R. B., Banner, J. L., Jobbágy, E. G., Pockman, W. T., & Wall, D. H. (2002). Ecosystem carbon loss with woody plant invasion of grasslands. *Nature*, 418(6898), 623–626.

Jurena, P. N. & Archer, S. (2003). Woody plant establishment and spatial heterogeneity in grasslands. *Ecology*, 84(4), 907–919.

Kangas, J. & Kohonen, T. (1996). Developments and applications of the self-organizing map and related algorithms. *Mathematics and Computers in Simulation*, 41(1-2), 3–12.

Karl, T. R., Gleason, B. E., Menne, M. J., McMahon, J. R., Heim, R. R., Brewer, M. J., Kunkel, K. E., Arndt, D. S., Privette, J. L., & Bates, J. J. (2012). US temperature and drought: Recent anomalies and trends. *Eos, Transactions American Geophysical Union*, 93(47), 473–474.

Katul, G., Kuhn, G., Schieldge, J., & Hsieh, C.-I. (1997). The ejection-sweep character of scalar fluxes in the unstable surface layer. *Boundary-Layer Meteorol*, 83(1), 1–26.

Katul, G., Poggi, D., Cava, D., & Finnigan, J. (2006). The relative importance of ejections and sweeps to momentum transfer in the atmospheric boundary layer. *Boundary-Layer Meteorol*, 120(3), 367–375.

Katul, G. G., Li, D., Chameki, M., & Bou-Zeid, E. (2013). Mean scalar concentration profile in a sheared and thermally stratified atmospheric surface layer. *Phys. Rev. E*, 87(2), 023004.

Knapp, A. K., Briggs, J. M., Collins, S. L., Archer, S. R., Bret-Harte, M. S., Ewers, B. E., Peters, D. P., Young, D. R., Shaver, G. R., Pendall, E., & Cleary, M. B. (2008). Shrub encroachment in North American grasslands: shifts in growth form dominance rapidly alters control of ecosystem carbon inputs. *Global Change Biol*, 14(3), 615–623.

Knapp, A. K., Briggs, J. M., & Koelliker, J. K. (2001). Frequency and Extent of Water Limitation to Primary Production in a Mesic Temperate Grassland. *Ecosystems*, 4(1), 19–28.

Kohonen, T. (1995). *Self-Organizing Maps*. Springer Series in Information Sciences. Springer Berlin Heidelberg.

Koster, R. D., Sud, Y. C., Guo, Z., Dirmeyer, P. A., Bonan, G., Oleson, K. W., Chan, E., Verseghy, D., Cox, P., & Davies, H. (2006). GLACE: the global land-atmosphere coupling experiment. Part I: overview. *J. Hydrometeor*, 7(4), 590–610.

Lawrence, D. M., Thornton, P. E., Oleson, K. W., & Bonan, G. B. (2007). The Partitioning of Evapotranspiration into Transpiration, Soil Evaporation, and Canopy Evaporation in a GCM: Impacts on Land–Atmosphere Interaction. *J. Hydrometeor*, 8(4), 862–880.

Lett, M. S., Knapp, A. K., Briggs, J. M., & Blair, J. M. (2004). Influence of shrub encroachment on aboveground net primary productivity and carbon and nitrogen pools in a mesic grassland. *Can. J. Bot.*, 82(9), 1363–1370.

Logan, K. E. & Brunsell, N. A. (2015). Agricultural and Forest Meteorology. *Agricultural and Forest Meteorology*, 213, 217–225.

Meyers, T. P. (2001). A comparison of summertime water and CO 2 fluxes over rangeland for well watered and drought conditions. *Agricultural and Forest Meteorology*, 106(3), 205–214.

Moene, A. F. & Schüttemeyer, D. (2008). The Effect of Surface Heterogeneity on the Temperature–Humidity Correlation and the Relative Transport Efficiency. *Boundary-Layer Meteorol*, 129(1), 99–113.

Moncrieff, J. B., Malhi, Y., & Leuning, R. (1996). The propogation of errors in long-term measurements of land–atmosphere fluxes of carbon and water. *Global Change Biol*, 2(3), 231–240.

Monin, A. S. & Obukhov, A. (1954). Basic laws of turbulent mixing in the surface layer of the atmosphere. *Contrib. Geophys. Inst. Acad. Sci. USSR*, 151, 163–187.

Nakagawa, H. & Nezu, I. (1977). Prediction of the contributions to the reynolds stress from bursting events in open-channel flows. *Journal of Fluid Mechanics*, 80(1), 99–128.

Nippert, J. B. & Knapp, A. K. (2007a). Linking water uptake with rooting patterns in grassland species. *Oecologia*, 153(2), 261–272.

Nippert, J. B. & Knapp, A. K. (2007b). Soil water partitioning contributes to species coexistence in tallgrass prairie. *Oikos*, 116(6), 1017–1029.

Nippert, J. B., Ocheltree, T. W., Skibbe, A. M., Kangas, L. C., Ham, J. M., Shonkwiler Arnold, K. B., & Brunsell, N. A. (2011). Linking plant growth responses across topographic gradients in tallgrass prairie. *Oecologia*, 166(4), 1131–1142.

Notaro, M. (2008). Statistical identification of global hot spots in soil moisture feedbacks among IPCC AR4 models. *J. Geophys. Res.*, 113(D9), 1490–8.

Orlowsky, B. & Seneviratne, S. I. (2010). Statistical Analyses of Land–Atmosphere Feedbacks and Their Possible Pitfalls. *J. Climate*, 23(14), 3918–3932.

Potts, D. L., Huxman, T. E., Scott, R. L., Williams, D. G., & Goodrich, D. C. (2006). The sensitivity of ecosystem carbon exchange to seasonal precipitation and woody plant encroachment. *Oecologia*, 150(3), 453–463.

Priestley, C. & Taylor, R. J. (1972). On the assessment of surface heat flux and evaporation using large-scale parameters. *Mon. Wea. Rev.*, 100(2), 81–92.

Ratajczak, Z., D'Odorico, P., Nippert, J. B., Collins, S. L., Brunsell, N. A., & Ravi, S. (2016). Changes in spatial variance during a grassland to shrubland state transition. *J Ecol*, 105(3), 750–760.

Ratajczak, Z., Nippert, J. B., & Collins, S. L. (2012). Woody encroachment decreases diversity across North American grasslands and savannas. *Ecology*, 93(4), 697–703.

Ratajczak, Z., Nippert, J. B., Hartman, J. C., & Ocheltree, T. W. (2011). Positive feedbacks amplify rates of woody encroachment in mesic tallgrass prairie. *Ecosphere*, 2(11), article 121.

Raupach, M. R. (2001). Combination theory and equilibrium evaporation. *Q.J.R. Meteorol. Soc.*, 127(574), 1149–1181.

Raupach, M. R., Finnigan, J. J., & Brunei, Y. (1996). Coherent eddies and turbulence in vegetation canopies: the mixing-layer analogy. *Boundary-Layer Meteorol*, 78(3-4), 351–382.

Reen, B. P., Stauffer, D. R., & Davis, K. J. (2014). Land-Surface Heterogeneity Effects in the Planetary Boundary Layer. *Boundary-Layer Meteorol*, 150(1), 1–31.

Reichstein, M., Falge, E., Baldocchi, D., Papale, D., Aubinet, M., Berbigier, P., Bernhofer, C., Buchmann, N., Gilmanov, T., Granier, A., et al. (2005). On the separation of net ecosystem exchange into assimilation and ecosystem respiration: review and improved algorithm. *Global Change Biology*, 11(9), 1424–1439.

Roundy, J. K., Ferguson, C. R., & Wood, E. F. (2013). Temporal Variability of Land–Atmosphere

Coupling and Its Implications for Drought over the Southeast United States. *J. Hydrometeor*, 14(2), 622–635.

Roundy, J. K., Ferguson, C. R., & Wood, E. F. (2014). Impact of land-atmospheric coupling in CFSv2 on drought prediction. *Climate Dynamics*, 43, 421–434.

Roundy, J. K. & Santanello, J. A. (2017). Utility of Satellite Remote Sensing for Land–Atmosphere Coupling and Drought Metrics. *J. Hydrometeor*, 18(3), 863–877.

Saintilan, N. & Rogers, K. (2014). Woody plant encroachment of grasslands: a comparison of terrestrial and wetland settings. *New Phytol*, 205(3), 1062–1070.

Santanello, J. A., Dirmeyer, P. A., Ferguson, C. R., Findell, K. L., Tawfik, A. B., Berg, A., Ek, M., Gentine, P., Guillod, B. P., van Heerwaarden, C., Roundy, J., & Wulfmeyer, V. (2017). Land-Atmosphere Interactions: The LoCo Perspective. *Bull. Amer. Meteor. Soc.*, (BAMS–D–17–0001).

Santanello, J. A., Kumar, S. V., Peters-Lidard, C. D., Harrison, K., & Zhou, S. (2013). Impact of Land Model Calibration on Coupled Land–Atmosphere Prediction. *J. Hydrometeor*, 14(5), 1373–1400.

Santanello, J. A., Peters-Lidard, C. D., & Kumar, S. V. (2011). Diagnosing the Sensitivity of Local Land–Atmosphere Coupling via the Soil Moisture–Boundary Layer Interaction. *J. Hydrometeor*, 12(5), 766–786.

Santanello, J. A., Peters-Lidard, C. D., Kumar, S. V., Alonge, C., & Tao, W.-K. (2009). A Modeling and Observational Framework for Diagnosing Local Land–Atmosphere Coupling on Diurnal Time Scales. *J. Hydrometeor*, 10(3), 577–599.

Santanello, J. A., Roundy, J., & Dirmeyer, P. A. (2015). Quantifying the Land–Atmosphere Coupling Behavior in Modern Reanalysis Products over the U.S. Southern Great Plains. *J. Climate*, 28(14), 5813–5829.

Scanlon, T. M. & Albertson, J. D. (2001). Turbulent transport of carbon dioxide and water vapor within a vegetation canopy during unstable conditions: Identification of episodes using wavelet analysis. *Journal of Geophysical Research: Atmospheres (1984–2012)*, 106(D7), 7251–7262.

Scanlon, T. M. & Kustas, W. P. (2010). Partitioning carbon dioxide and water vapor fluxes using correlation analysis. *Agricultural and Forest Meteorology*, 150(1), 89–99.

Schwalm, C. R., Williams, C. A., Schaefer, K., Arneth, A., Bonal, D., Buchmann, N., Chen, J., Law, B. E., Lindroth, A., Luyssaert, S., Reichstein, M., & Richardson, A. D. (2010). Assimilation exceeds respiration sensitivity to drought: A FLUXNET synthesis. *Global Change Biol*, 16(2), 657–670.

Scott, R. L., Huxman, T. E., Williams, D. G., & Goodrich, D. C. (2006). Ecohydrological impacts of woody-plant encroachment: seasonal patterns of water and carbon dioxide exchange within a semiarid riparian environment. *Global Change Biol*, 12(2), 311–324.

Seneviratne, S. I., Corti, T., Davin, E. L., Hirschi, M., Jaeger, E. B., Lehner, I., Orlowsky, B., & Teuling, A. J. (2010). Investigating soil moisture–climate interactions in a changing climate: A review. *Earth Science Reviews*, 99(3-4), 125–161.

Spennemann, P. C. & Saulo, A. C. (2015). An estimation of the land-atmosphere coupling strength in South America using the Global Land Data Assimilation System. *Int. J. Climatol.*, 35(14), 4151–4166.

Sun, S. & Wang, G. (2012). The complexity of using a feedback parameter to quantify the soil moisture-precipitation relationship. *J. Geophys. Res. Atmos.*, 117, D11113.

Trenberth, K. E., Fasullo, J. T., & Kiehl, J. (2009). Earth's Global Energy Budget. *Bull. Amer. Meteor. Soc.*, 90(3), 311–323.

van Heerwaarden, C. C., Vilà-Guerau de Arellano, J., Moene, A. F., & Holtslag, A. A. M. (2009).

Interactions between dry-air entrainment, surface evaporation and convective boundary-layer development. *Q.J.R. Meteorol. Soc.*, 135, 1277–1291.

Wei, J., Dirmeyer, P. A., Wisser, D., Bosilovich, M. G., & Mocko, D. M. (2013). Where Does the Irrigation Water Go? An Estimate of the Contribution of Irrigation to Precipitation Using MERRA. *J. Hydrometeor*, 14(1), 275–289.

Williams, C. A., Scanlon, T. M., & Albertson, J. D. (2006). Influence of surface heterogeneity on scalar dissimilarity in the roughness sublayer. *Boundary-Layer Meteorol*, 122(1), 149–165.

Wohlfahrt, G., Anfang, C., Bahn, M., Haslwanter, A., Newesely, C., Schmitt, M., Drösler, M., Pfadenhauer, J., & Cernusca, A. (2005). Quantifying nighttime ecosystem respiration of a meadow using eddy covariance, chambers and modelling. *Agricultural and Forest Meteorology*, 128(3-4), 141–162.

Wolf, S., Keenan, T. F., Fisher, J. B., Baldocchi, D. D., Desai, A. R., RICHARDSON, A. D., Scott, R. L., LAW, B. E., Litvak, M. E., Brunsell, N. A., Peters, W., & van der Laan-Luijkx, I. T. (2016). Warm spring reduced carbon cycle impact of the 2012 US summer drought. *Proceedings of the National Academy of Sciences*, (pp. 5880–5885).

Wyngaard, J. C., Coté, O. R., & Izumi, Y. (1971). Local free convection, similarity, and the budgets of shear stress and heat flux. *J. Atmos. Sci.*, 28(7), 1171–1182.

Zaitchik, B. F., Santanello, J. A., Kumar, S. V., & Peters-Lidard, C. D. (2013). Representation of Soil Moisture Feedbacks during Drought in NASA Unified WRF (NU-WRF). *J. Hydrometeor*, 14(1), 360–367.

Zeng, X., Barlage, M., Castro, C., & Fling, K. (2010). Comparison of Land–Precipitation Coupling Strength Using Observations and Models. *J. Hydrometeor*, 11(4), 979–994.

Zhang, J., Wang, W.-C., & Wei, J. (2008). Assessing land-atmosphere coupling using soil moisture

from the Global Land Data Assimilation System and observational precipitation. *J. Geophys. Res.*, 113(D17), 5024–14.

Zhang, J., Wang, W.-C., & Wu, L. (2009). Land-atmosphere coupling and diurnal temperature range over the contiguous United States. *Geophys. Res. Lett.*, 36(6), 1697–5.